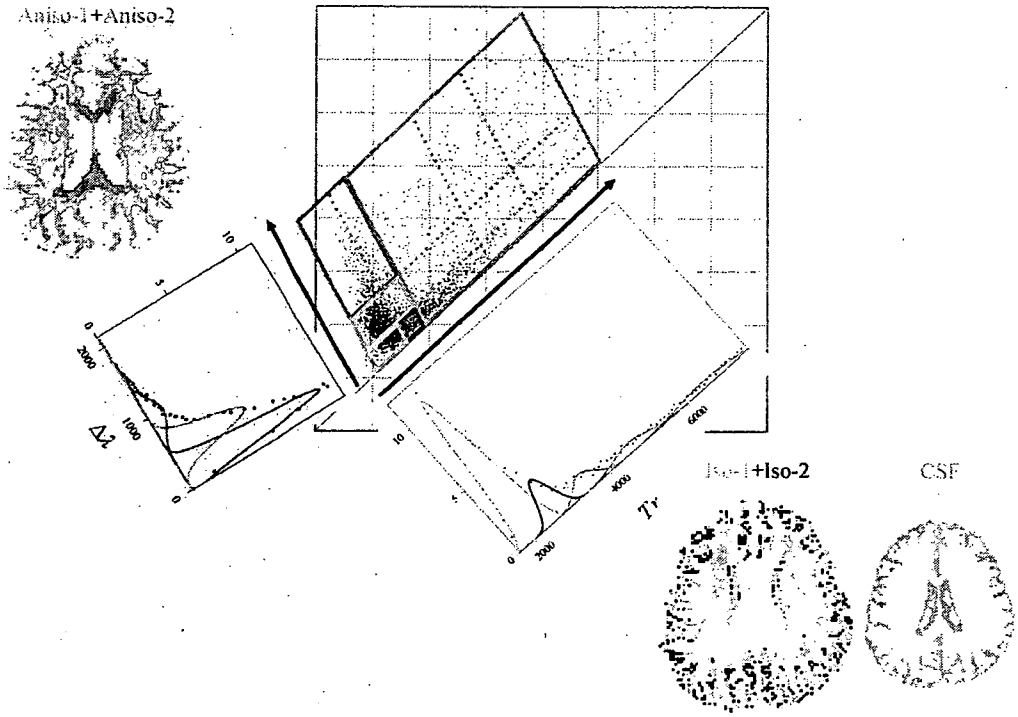

Fig. 2. Data analysis. For partitioning all the pixels on the lambda chart using the parallelogram compartments shown here, the ranges of the two parameters, namely, $Tr=\lambda_L+2\lambda_T$ and $\Delta\lambda=\lambda_L-\lambda_T$ must be determined. On the nonorthogonal coordinate system of Tr versus $\Delta\lambda$, all the pixels on the lambda chart when plotted against their Tr created a Tr function, and also a $\Delta\lambda$ function when plotted against their $\Delta\lambda$. By nonlinear least-squares curve-fitting processes using a multiple Gaussian mixture model, the Tr function was deconvolved into five Gaussian elements and the $\Delta\lambda$ function into three elements. Hence, the two-dimensional Gaussian deconvolution on the coordinate system of Tr versus $\Delta\lambda$ specified 5×3 pixel groups with unique ranges of Tr and $\Delta\lambda$ values, as shown by the dotted parallelogram compartments on the lambda chart. By remapping the pixels belonging to each compartment back onto the image matrix, 5×3 pictorial images of the compartments were created. By assessing the anatomical distribution of these images, the 5×3 pixel compartments were integrated into five pixel components (i.e., Iso-1, Iso-2, Aniso-1, Aniso-2, and CSF), which are shown as solid parallelogram compartments on the chart and as three types of pictorial image (i.e., Iso-1+Iso-2, Aniso-1+Aniso-2, and CSF).

ventricles, sulcus and cisterns. Similarly, the deconvolution of the $\Delta\lambda$ function into three Gaussian elements gave sufficient ranges of the $\Delta\lambda$ values for segregating NABT excluding CSF. Although these deconvolutions also provide sufficient resolution for segregating NABT excluding CSF, further deconvolution may be possible by improving the accuracy of these functions.

The Gaussian deconvolutions of the Tr and $\Delta\lambda$ functions provided five ranges of nonoverlapping Tr values and three ranges of nonoverlapping $\Delta\lambda$ values, respectively. Therefore, the two-dimensional deconvolution of these two functions in the coordinate system of Tr versus $\Delta\lambda$ specified 5×3 pixel compartments that have unique ranges of Tr and $\Delta\lambda$ values, as shown by the dotted parallelograms on the lambda chart (Fig. 2).

Determination of pixel components corresponding to NABT for numerical analysis

By remapping the pixels belonging to each of the specified 5×3 compartments back onto the original image matrix, 5×3 pictorial images of the compartments were created. By assessing the anatomical distribution of these images, the 5×3 compartments were integrated into the following five pixel components, as shown by the solid parallelograms on the lambda chart and the pictorial images of the same color (Fig. 2). In the isotropic part on the lambda chart, there were two components, namely, Iso-1 and Iso-2. Iso-1, as shown by the light blue pictorial image, corresponded to structures primarily composed of relatively small neurons and glia; Iso-2, as shown by the blue pictorial image, corresponded to structures primarily containing numerous large neurons. The anisotropic part on the lambda chart was composed of two components, namely, Aniso-1 and Aniso-2. Aniso-1, as shown by the orange pictorial image, corresponded to structures primarily composed of relatively short axons creating short tracts; Aniso-2, as shown by the orange–red pictorial image, corresponded to structures primarily containing relatively long axons creating long tracts. The component shown as a solid dark gray parallelogram on the lambda chart, which was composed of nine dotted parallelograms, corresponded to structures mainly containing CSF in the cortical sulci, ventricles and cisterns, as shown by the dark gray pictorial image. The pixels containing CSF with higher diffusivity could not be classified into any of these components and therefore were not shown as a pictorial image.

Subsequently, the four components excluding CSF (i.e., Iso-1, Iso-2, Aniso-1, and Aniso-2) were subjected to statistical inference for the following parameters: the volume fraction of each component to the whole brain of a slice, and the mean values of DTI-derived parameters of all the pixels belonging to each component (i.e., Tr, FA, λ_L, and λ_T). Statistical inferences were performed using Statistica 2000 (StatSoft Inc., Tulsa, OK, USA). The differences in each parameter between the healthy volunteers and the RRMS patients were compared using Welch's nonpaired *t* test, with the overall alpha level set at 0.05.

Results

Fig. 3 shows a representative set of pixel component images in a pictorial form of a healthy volunteer and a patient with RRMS. The volumes of the anisotropic components (Aniso-1 and Aniso-2) of the RRMS patient appear to be lower than those of the healthy volunteer (Fig. 3C). In contrast, the volumes of the isotropic components (Iso-1 and Iso-2) of the patient seem to be higher than those of the healthy volunteer (Fig. 3B). These visual impressions were confirmed by the numerical analyses of the components (Table 2). The volume fractions of Aniso-1 in the RRMS patients were markedly smaller than those in the healthy volunteers, and the volume fractions of Iso-1 were significantly larger in the RRMS patients than those in the healthy volunteers. The numerical analyses also showed that in all of the four components, Tr values were markedly higher and FA values were significantly lower in the RRMS patients than those in the healthy volunteers. Additionally, in all of the four components, both λ_L and λ_T values in the RRMS patients were significantly higher than those in the healthy volunteers, except for λ_L values in Aniso-2.

Discussion

The method of segmenting brain tissue used in this study is based on the concept that the partitioning of the pixels on a scatter plot of two DTI-derived parameters enables the anatomical segmentation of the brain structure, which has been found in a previous work (Pierpaoli et al., 1996). Furthermore, our method has the following three unique features that have not been reported in other previous segmentation methods.

The first feature is the characteristic of LCA *per se*: the segregation of pixel groups is processed solely from the diffusion characteristics of each pixel provided by LCA and is totally independent of information regarding pixel position on the image matrix. In other words, our segmentation method does not require any spatial information given by structural images. This enables a more accurate segmentation in each subject than other methods that require spatial normalization using a structural image template. In addition, segmenting the gray or white matter further into more detailed anatomical structures is difficult using the structural image template alone (Rashid et al., 2004).

The second feature is that the criteria for segmentation in our method are not given a priori as fixed cutoff values, but are provided a posteriori by the two-dimensional Gaussian deconvolution in each subject. This allows for a more flexible segmentation of the brain tissue, even if the target tissues are damaged to change their diffusion characteristics, than a previous method using a fixed FA as the cutoff value for segmenting the gray matter and white matter (Cercignani et al., 2001a).

The final feature is that, as a result of the Gaussian deconvolution, the parameters of the diffusion characteristics of the segmented pixel components are normally distributed except for the overlapped tails of the Gaussian distributions, which allows the use of parametric statistical inferences by considering the results of

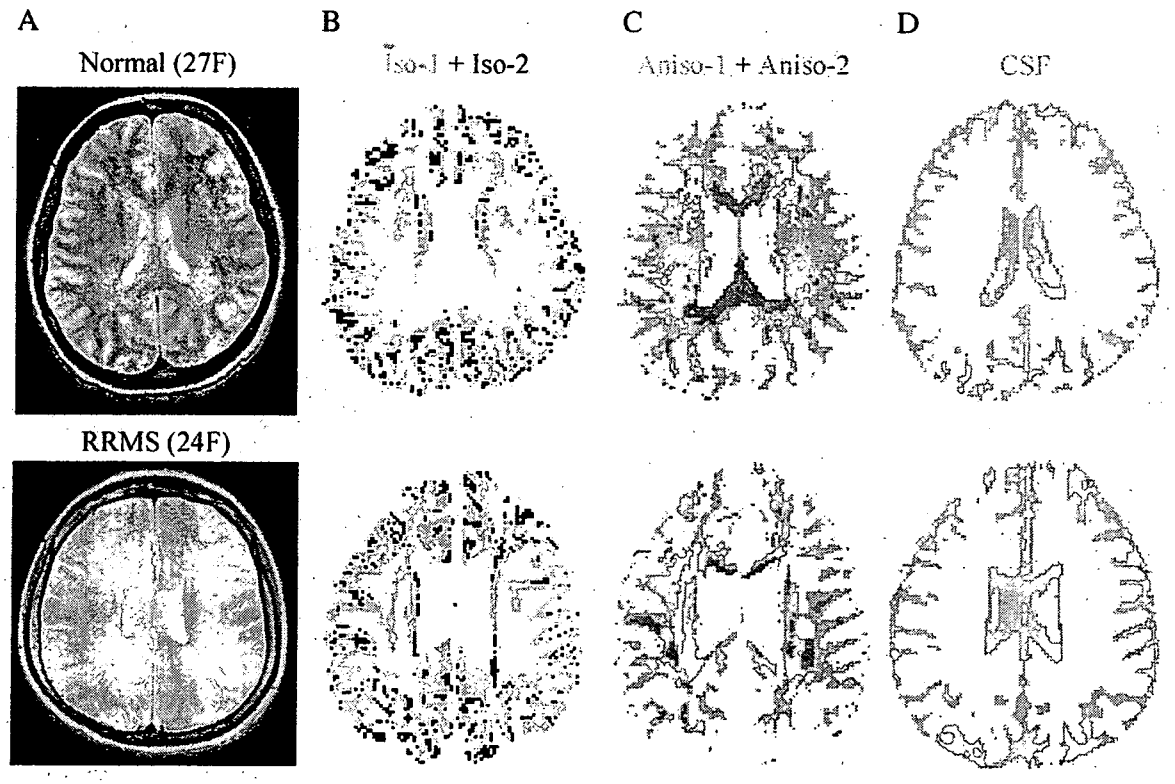

Fig. 3. Representative set of pixel component images in pictorial form of healthy volunteer (upper) and patient with remitting–relapsing multiple sclerosis (RRMS, lower). (A) fast spin-echo images; (B) isotropic pixel components (Iso-1 and Iso-2); (C) anisotropic pixel components (Aniso-1 and Aniso-2); (D) cerebrospinal fluid (CSF) in cortical sulci, cisterns, and ventricles. The volumes of the anisotropic components of the RRMS patient appear to be lower than those of the healthy volunteer, as shown in C. In contrast, the volumes of the isotropic components of the RRMS patient seem to be higher than those of the healthy volunteer, as shown in B.

Table 2
Numerical analyses of each pixel component

	Control	RRMS
Iso-1		
Volume fraction	0.22±0.04	0.26±0.03†
Tr ($\times 10^{-3}$ mm^2/s)	2.17±0.05	2.30±0.12†
FA	0.24±0.02	0.22±0.02†
λ_L ($\times 10^{-3}$ mm^2/s)	0.89±0.02	0.98±0.04†
λ_T ($\times 10^{-3}$ mm^2/s)	0.64±0.02	0.68±0.04†
Iso-2		
Volume fraction	0.10±0.03	0.10±0.01
Tr ($\times 10^{-3}$ mm^2/s)	2.71±0.09	2.89±0.22†
FA	0.17±0.01	0.16±0.02†
λ_L ($\times 10^{-3}$ mm^2/s)	1.05±0.03	1.11±0.07†
λ_T ($\times 10^{-3}$ mm^2/s)	0.83±0.03	0.89±0.07†
Aniso-1		
Volume fraction	0.34±0.04	0.29±0.03†
Tr ($\times 10^{-3}$ mm^2/s)	2.24±0.04	2.39±0.14†
FA	0.44±0.02	0.41±0.03†
λ_L ($\times 10^{-3}$ mm^2/s)	1.12±0.02	1.16±0.05†
λ_T ($\times 10^{-3}$ mm^2/s)	0.57±0.02	0.62±0.05†
Aniso-2		
Volume fraction	0.05±0.01	0.05±0.02
Tr ($\times 10^{-3}$ mm^2/s)	2.41±0.06	2.53±0.17†
FA	0.68±0.03	0.63±0.05†
λ_L ($\times 10^{-3}$ mm^2/s)	1.55±0.07	1.55±0.08
λ_T ($\times 10^{-3}$ mm^2/s)	0.43±0.03	0.49±0.03†

Values represent means±standard deviations.
Volume fraction=volume fraction of each component to whole brain of slice; Tr=mean value of trace in each component; FA=mean of fractional anisotropy; λ_L=mean of lambda longitudinal; λ_T=mean of lambda transverse.
† Significantly different from controls ($P<0.05$, Welch's nonpaired t test).

the chi-square tests for these parameters. This indicates that the mean and the standard deviation of the DTI-derived parameter are necessary and sufficient statistics to represent its distribution. In previous studies using histogram analysis, the peak height and peak location of the histogram were used for statistical inferences, probably because the target parameters such as FA and MD in these studies did not exhibit a normal distribution. However, in general, the parameters considered to show a normal distribution are more easily analyzed statistically.

On the other hand, some technical limitations in our segmentation algorithm were observed. The most critical problem is the underestimation of the diffusion anisotropy of a pixel containing crossing or diverging tracts. This phenomenon can be observed using not only our method based on the lambda chart analysis but also other methods generally used in DTI for determining only one principal direction of diffusion anisotropy within a pixel. In such methods, pixels containing crossing or diverging tracts can be misclassified to the component showing lower diffusion anisotropy than what each tract actually shows. Therefore, a pixel that is supposed to belong to Aniso-2 can be misclassified to Aniso-1, or a pixel that is supposed to belong to Aniso-1 can be misclassified to Iso-1 or Iso-2. A good example is the pixels containing the motor tracts in the corona radiata. Although the motor tracts are supposed to belong to Aniso-2 corresponding to long tracts, these pixels are shown as Aniso-1, whereas the pixels containing the motor tracts at a lower slice level of the posterior limbs of the internal capsules are obviously shown as Aniso-2, because the motor tracts at this slice level run in an almost uniform direction (Fig. 4). This misclassification problem may be solved using alternative methods of measurement of diffusion anisotropy, such as High Angular Resolution Diffusion Imaging (HARDI) (Tuch et al., 2002) or q-space imaging (Assaf and Cohen, 2000), which remain to be investigated in the future.

Another problem is the existence of an overlap of two neighboring Gaussian elements. This overlapped portion assigned to one Gaussian element may actually belong to the other Gaussian element. Although the overlapped portion slightly affected the overall results of the analyses of NABT injury in this study, this problem can lead to another type of misclassification problem, which is difficult to resolve only with information provided by DTI. In spite of these present limitations, we believe that the success of this study for analyzing NABT injury in MS was largely due to the unique features of the segmentation algorithms described above.

The analyses of the two anisotropic components Aniso-1 and Aniso-2 showed the detailed pathology of NAWM injury. Both Aniso-1 and Aniso-2 of the RRMS patients had higher Tr values and

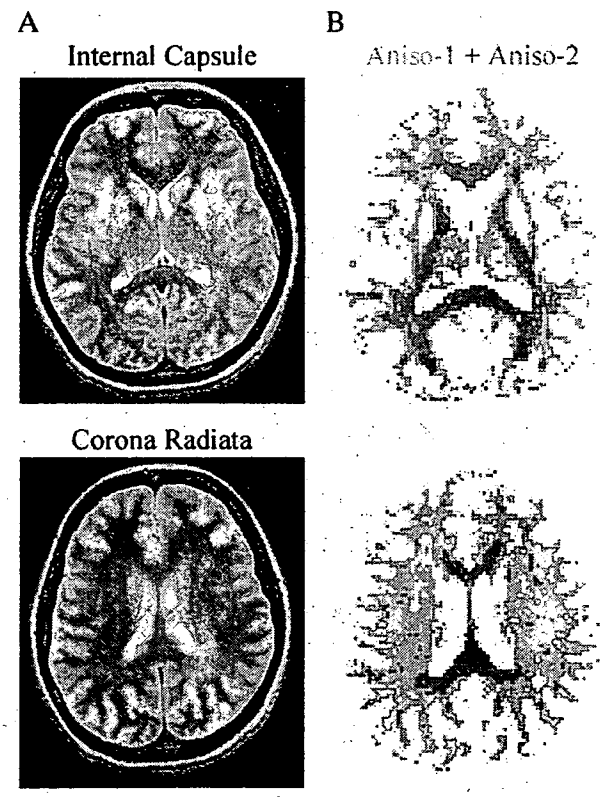

Fig. 4. Misclassified motor tracts at slice level of internal capsule (upper) and corona radiata (lower) of healthy volunteer. A: fast spin-echo images; B: anisotropic pixel components (Aniso-1 and Aniso-2). Note the pixels containing motor tracts passing through the posterior limbs of the internal capsule. These pixels are clearly shown as orange–red Aniso-2 corresponding to long tracts (upper), whereas the pixels containing the motor tracts in the corona radiata are shown as orange Aniso-1 (lower). This phenomenon is due to the misclassification of the pixels containing the diverging motor tracts in the corona radiata.

lower FA values than those of the healthy volunteers, which are in agreement with those of previous DTI studies evaluating NAWM injury in MS patients (Werring et al., 1999; Bammer et al., 2000; Filippi et al., 2001; Ciccarelli et al., 2001). In addition, the individual analyses of the changes in λ_L and λ_T values (Suzuki et al., 2003), which are useful for evaluating more detailed changes in the diffusion characteristics, indicated that the observed increase in the Tr values resulted from the increases in both λ_L and λ_T values, and that the decrease in the FA values resulted from a relatively larger increase in λ_T values than in λ_L values. These results showed that 1) the increase in the Tr values, suggesting increased diffusivity, was due to an increase in the unrestricted water content in the extraaxonal space, and that 2) the decrease in the FA value, suggesting decreased diffusion anisotropy, resulted from the disintegration of the axonal structure, such as axonal loss and demyelination. Diffuse astrocytic hyperplasia, patchy edema, perivascular infiltration, gliosis, an abnormally thin myelin, and axonal loss, all of which are observed in NAWM in MS (Allen and McKeown, 1979), led to the changes in these DTI-derived parameters.

Furthermore, the analyses of the anisotropic components showed that the volume fractions of Aniso-1 were markedly decreased but those of Aniso-2 were not significantly decreased in the RRMS patients compared with those of the healthy volunteers. The visible MS plaque lesions in the patients were all very small to account for these changes in the white matter volume by considering their volume fractions, as shown in Table 1. Therefore, it is reasonable to assume that the changes in the white matter volume, which were more severe in Aniso-1 than in Aniso-2 in this study, resulted from the NAWM injury such as axonal loss. These results are highly consistent with those of previous histological studies showing that small fibers are more vulnerable than large fibers in MS (Ganter et al., 1999; Evangelou et al., 2001). To the best of our knowledge, our study is the first MR-based study to substantiate this histological observation of NAWM injury.

The analyses of the two isotropic components Iso-1 and Iso-2 also demonstrated important findings of NAGM injury in MS. Similar to the results of the anisotropic components, both Iso-1 and Iso-2 of the RRMS patients had higher Tr values and lower FA values than those of the healthy volunteers, which are in agreement with those of previous DTI studies evaluating NAGM injury in MS (Cercignani et al., 2001a; Bozzali et al., 2002; Rovaris et al., 2002). Furthermore, our study demonstrated that more marked changes in DTI-derived parameters were observed in the RRMS patients in spite of the fact that these patients had relatively mild disabilities, as shown by EDSS less than or equal to 3.5, than in patients in previous studies. This is probably due to the advantages of our segmentation methods for NAGM in MS over these previous methods.

In addition, the analyses of the isotropic components showed that the volume fractions of Iso-1 in the RRMS patients were significantly *higher* than those in the healthy volunteers. We think that two factors were likely to be involved in this phenomenon: one was the actual enlargement of Iso-1 resulting from gliosis or hypertrophic astrocytosis in NAGM, and the other was that pixels belonging formerly to Aniso-1 lost their diffusion anisotropy during the disease process, and were consequently resegregated into Iso-1. Therefore, the component Iso-1 in the RRMS patients is considered to include injured short axons primarily located in the subcortical white matter, as well as small neurons and proliferating glial cells primarily located in the cortical deep layer, all of which showed increased diffusivity and decreased diffusion anisotropy. Hence, the component Iso-1 is considered to correspond to the "juxtacortical region", which previous histological studies showed to be the most vulnerable site in MS (Brownell and Hughes, 1962; Kidd et al., 1999). Our study is again the first MR-based study *in vivo* to substantiate this histological observation of NAGM injury, although a previous study demonstrated similar findings using *postmortem* MR imaging (Geurts et al., 2005).

In conclusion, our study not only supports the results of previous DTI studies evaluating NABT injury in MS, but also clarified the pathology of NAGM/NAWM injury at the cellular level *in vivo*, which is similar to that obtained by histological examination. We expect that our method will further elucidate the details of the pathogenesis of MS, which will be of great help for predicting the prognosis of MS patients or for deciding their therapeutic regimens.

Acknowledgments

This study was supported by grants from the Ministry of Education, Culture, Sports, Science and Technology (Japan) and a grant from the Japan Multiple Sclerosis Society. The author (Kenshi Terajima) received financial support for research activities from Bayer Yakuhin Ltd. (former Nihon Schering K.K.).

We wish to acknowledge the helpful discussions with Dr. Masami Tanaka (Department of Neurology, Utano National Hospital, Kyoto, Japan) in the course of this study.

References

Allen, I.V., McKeown, S.R., 1979. A histological, histochemical and biochemical study of the macroscopically normal white matter in multiple sclerosis. J. Neurol. Sci. 41, 81–91.

Assaf, Y., Cohen, Y., 2000. Assignment of the water slow-diffusing component in the central nervous system using q-space diffusion MRS: implications for fiber tract imaging. Magn. Reson. Med. 43, 191–199.

Bammer, R., Augustin, M., Strasser-Fuchs, S., Seifert, T., Kapeller, P., Stollberger, R., Ebner, F., Hartung, H.P., Fazekas, F., 2000. Magnetic resonance diffusion tensor imaging for characterizing diffuse and focal white matter abnormalities in multiple sclerosis. Magn. Reson. Med. 44, 583–591.

Bjartmar, C., Kinkel, R.P., Kidd, G., Rudick, R.A., Trapp, B.D., 2001. Axonal loss in normal-appearing white matter in a patient with acute MS. Neurology 57, 1248–1252.

Bozzali, M., Cercignani, M., Sormani, M.P., Comi, G., Filippi, M., 2002. Quantification of brain gray matter damage in different ms phenotypes by use of diffusion tensor MR imaging. AJNR Am. J. Neuroradiol. 23, 985–988.

Brownell, B., Hughes, J.T., 1962. The distribution of plaques in the cerebrum in multiple sclerosis. J. Neurol. Neurosurg. Psychiatry 25, 315–320.

Cercignani, M., Bozzali, M., Iannucci, G., Comi, G., Filippi, M., 2001a. Magnetisation transfer ratio and mean diffusivity of normal appearing white and grey matter from patients with multiple sclerosis. J. Neurol. Neurosurg. Psychiatry 70, 311–317.

Cercignani, M., Inglese, M., Pagani, E., Comi, G., Filippi, M., 2001b. Mean diffusivity and fractional anisotropy histograms of patients with multiple sclerosis. AJNR Am. J. Neuroradiol. 22, 952–958.

Ciccarelli, O., Werring, D.J., Wheeler-Kingshott, C.A., Barker, G.J., Parker, G.J., Thompson, A.J., Miller, D.H., 2001. Investigation of MS normal-appearing brain using diffusion tensor MRI with clinical correlations. Neurology 56, 926–933.

De Stefano, N., Matthews, P.M., Fu, L., Narayanan, S., Stanley, J., Francis, G.S., Antel, J.P., Arnold, D.L., 1998. Axonal damage correlates with

disability in patients with relapsing–remitting multiple sclerosis. Results of a longitudinal magnetic resonance spectroscopy study. Brain 121, 1469–1477.

Evangelou, N., Konz, D., Esiri, M.M., Smith, S., Palace, J., Matthews, P.M., 2000. Regional axonal loss in the corpus callosum correlates with cerebral white matter lesion volume and distribution in multiple sclerosis. Brain 123, 1845–1849.

Evangelou, N., Konz, D., Esiri, M.M., Smith, S., Palace, J., Matthews, P.M., 2001. Size-selective neuronal changes in the anterior optic pathways suggest a differential susceptibility to injury in multiple sclerosis. Brain 124, 1813–1820.

Filippi, M., Iannucci, G., Tortorella, C., Minicucci, L., Horsfield, M.A., Colombo, B., Sormani, M.P., Comi, G., 1999. Comparison of MS clinical phenotypes using conventional and magnetization transfer MRI. Neurology 52, 588–594.

Filippi, M., Cercignani, M., Inglese, M., Horsfield, M.A., Comi, G., 2001. Diffusion tensor magnetic resonance imaging in multiple sclerosis. Neurology 56, 304–311.

Ganter, P., Prince, C., Esiri, M.M., 1999. Spinal cord axonal loss in multiple sclerosis: a post-mortem study. Neuropathol. Appl. Neurobiol. 25, 459–467.

Geurts, J.J., Bo, L., Pouwels, P.J., Castelijns, J.A., Polman, C.H., Barkhof, F., 2005. Cortical lesions in multiple sclerosis: combined postmortem MR imaging and histopathology. AJNR Am. J. Neuroradiol. 26, 572–577.

Kalkers, N.F., Hintzen, R.Q., van Waesberghe, J.H., Lazeron, R.H., van Schijndel, R.A., Adèr, H.J., Polman, C.H., Barkhof, F., 2001. Magnetization transfer histogram parameters reflect all dimensions of MS pathology, including atrophy. J. Neurol. Sci. 184, 155–162.

Kidd, D., Barkhof, F., McConnell, R., Algra, P.R., Allen, I.V., Revesz, T., 1999. Cortical lesions in multiple sclerosis. Brain 122, 17–26.

Kurtzke, J.F., 1983. Rating neurologic impairment in multiple sclerosis: an expanded disability status scale (EDSS). Neurology 33, 1444–1452.

Lumsden, C.E., 1970. The neuropathology of multiple sclerosis. In: Vinken, P.J., Bruyn, G.W. (Eds.), Handbook of Clinical Neurology, vol. 9. North-Holland, Amsterdam, pp. 217–309.

Matsuzawa, H., Nakada, T., 2000. Lambda chart analysis and eigenvalue imaging. In: Nakada, T. (Ed.), Integrated Human Brain Science: Theory, Method Application (Music). Elsevier Science B.V., Amsterdam, pp. 219–225.

Matsuzawa, H., Nakayama, N., Kwee, I.L., Nakada, T., 2005. Isotropic component trace analysis. Journal of Neuroimaging 15, 233–239.

Nusbaum, A.O., Tang, C.Y., Wei, T., Buchsbaum, M.S., Atlas, S.W., 2000. Whole-brain diffusion MR histograms differ between MS subtypes. Neurology 54, 1421–1427.

Pierpaoli, C., Jezzard, P., Basser, P.J., Barnett, A., Di Chiro, G., 1996. Diffusion tensor MR imaging of the human brain. Radiology 201, 637–648.

Polman, C.H., Reingold, S.C., Edan, G., Filippi, M., Hartung, H.P., Kappos, L., Lublin, F.D., Metz, L.M., McFarland, H.F., O'Connor, P.W., Sandberg-Wollheim, M., Thompson, A.J., Weinshenker, B.G., Wolinsky, J.S., 2005. Diagnostic criteria for multiple sclerosis: 2005 revisions to the "McDonald Criteria". Ann. Neurol. 58, 840–846.

Rashid, W., Hadjiprocopis, A., Griffin, C.M., Chard, D.T., Davies, G.R., Barker, G.J., Tofts, P.S., Thompson, A.J., Miller, D.H., 2004. Diffusion tensor imaging of early relapsing–remitting multiple sclerosis with histogram analysis using automated segmentation and brain volume correction. Mult. Scler. (Houndmills, Basingstoke, England) 10, 9–15.

Rovaris, M., Filippi, M., Falautano, M., Minicucci, L., Rocca, M.A., Martinelli, V., Comi, G., 1998. Relation between MR abnormalities and patterns of cognitive impairment in multiple sclerosis. Neurology 50, 1601–1608.

Rovaris, M., Bozzali, M., Iannucci, G., Ghezzi, A., Caputo, D., Montanari, E., Bertolotto, A., Bergamaschi, R., Capra, R., Mancardi, G.L., Martinelli, V., Comi, G., Filippi, M., 2002. Assessment of normal-appearing white and gray matter in patients with primary progressive multiple sclerosis: a diffusion-tensor magnetic resonance imaging study. Arch. Neurol. 59, 1406–1412.

Santos, A.C., Narayanan, S., de Stefano, N., Tartaglia, M.C., Francis, S.J., Arnaoutelis, R., Caramanos, Z., Antel, J.P., Pike, G.B., Arnold, D.L., 2002. Magnetization transfer can predict clinical evolution in patients with multiple sclerosis. J. Neurol. 249, 662–668.

Suzuki, Y., Matsuzawa, H., Kwee, I.L., Nakada, T., 2003. Absolute eigenvalue diffusion tensor analysis for human brain maturation. NMR Biomed. 16, 257–260.

Tanaka, K., Tani, T., Tanaka, M., Saida, T., Idezuka, J., Yamazaki, M., Tsujita, M., Nakada, T., Sakimura, K., Nishizawa, M., 2007. Anti-aquaporin 4 antibody in Japanese multiple sclerosis with long spinal cord lesions. Mult. Scler. (Houndmills, Basingstoke, England).

Tuch, D.S., Reese, T.G., Wiegell, M.R., Makris, N., Belliveau, J.W., Wedeen, V.J., 2002. High angular resolution diffusion imaging reveals intravoxel white matter fiber heterogeneity. Magn. Reson. Med. 48, 577–582.

van Buchem, M.A., McGowan, J.C., Kolson, D.L., Polansky, M., Grossman, R.I., 1996. Quantitative volumetric magnetization transfer analysis in multiple sclerosis: estimation of macroscopic and microscopic disease burden. Magn. Reson. Med. 36, 632–636.

van Buchem, M.A., Grossman, R.I., Armstrong, C., Polansky, M., Miki, Y., Heyning, F.H., Boncoeur-Martel, M.P., Wei, L., Udupa, J.K., Grossman, M., Kolson, D.L., McGowan, J.C., 1998. Correlation of volumetric magnetization transfer imaging with clinical data in MS. Neurology 50, 1609–1617.

Werring, D.J., Clark, C.A., Barker, G.J., Thompson, A.J., Miller, D.H., 1999. Diffusion tensor imaging of lesions and normal-appearing white matter in multiple sclerosis. Neurology 52, 1626–1632.

Zivadinov, R., Sepcic, J., Nasuelli, D., De Masi, R., Bragadin, L.M., Tommasi, M.A., Zambito-Marsala, S., Moretti, R., Bratina, A., Ukmar, M., Pozzi-Mucelli, R.S., Grop, A., Cazzato, G., Zorzon, M., 2001. A longitudinal study of brain atrophy and cognitive disturbances in the early phase of relapsing–remitting multiple sclerosis. J. Neurol. Neurosurg. Psychiatry 70, 773–780.

Resistance to Experimental Autoimmune Encephalomyelitis and Impaired T Cell Priming by Dendritic Cells in Src Homology 2 Domain-Containing Protein Tyrosine Phosphatase Substrate-1 Mutant Mice[1]

Takeshi Tomizawa,[2]* Yuka Kaneko,[2†‡] Yoriaki Kaneko,[3]* Yasuyuki Saito,* Hiroshi Ohnishi,† Jun Okajo,* Chie Okuzawa,* Tomomi Ishikawa-Sekigami,* Yoji Murata,† Hideki Okazawa,† Koichi Okamoto,‡ Yoshihisa Nojima,* and Takashi Matozaki[3†]

Src homology 2 domain-containing protein tyrosine phosphatase (SHP) substrate-1 (SHPS-1) is a transmembrane protein that binds the protein tyrosine phosphatases SHP-1 and SHP-2 through its cytoplasmic region and is expressed on the surface of CD11c dendritic cells (DCs) and macrophages. In this study, we show that mice that express a mutant form of SHPS-1 lacking most of the cytoplasmic region are resistant to experimental autoimmune encephalomyelitis (EAE) in response to immunization with a peptide derived from myelin oligodendrocyte glycoprotein (MOG (35o55)). The MOG (35o55)-induced proliferation of, and production of IFN- , IL-2, and IL-17, by T cells from immunized SHPS-1 mutant mice were reduced compared with those apparent for wild-type cells. The abilities of splenic DCs from mutant mice to stimulate an allogenic MLR and to prime Ag-specific T cells were reduced. Both IL-12-stimulated and TLR-dependent cytokine production by DCs of mutant mice were also impaired. Finally, SHPS-1 mutant mice were resistant to induction of EAE by adoptive transfer of MOG (35o55)-specific T cells. These results show that SHPS-1 on DCs is essential for priming of naive T cells and the development of EAE. SHPS-1 is thus a potential therapeutic target in inflammatory disorders of the CNS and other autoimmune diseases. *The Journal of Immunology,* **2007, 179: 869o877.**

Dendritic cells (DCs)[4] are professional APCs and play a central role in the induction of immune responses to pathogens (1, 2). When immature DCs, such as Langerhans cells, which reside in nonlymphoid tissues, encounter exogenous Ags, they engulf and process them for presentation of Ag-derived peptides in complexes with MHC molecules on the cell surface. The DCs subsequently migrate to draining lymph nodes (LNs) and make contact with naive T cells. During such migration, DCs mature and express costimulatory molecules such as CD80, CD86, and CD40 in addition to MHC class II molecules on their surface. The mature DCs thus present MHC-peptide complexes to naive T cells together with costimulatory molecules that are essential for priming of the T cells by DCs (3). However, the detailed molecular mechanism of priming of naive T cells by DCs remains largely unknown.

Src homology 2 domain-containing protein tyrosine phosphatase (SHP) substrate-1 (SHPS-1) (4), also known as signal-regulatory protein (5, 6) or brain Ig-like molecule with tyrosine-based activation motifs (BIT) (7), is a transmembrane protein whose extracellular region comprises three Ig-like domains and whose cytoplasmic region contains four tyrosine phosphorylation sites that mediate the binding of the protein tyrosine phosphatases SHP-1 and SHP-2. Tyrosine phosphorylation of SHPS-1 is regulated by various growth factors and cytokines as well as by integrin-mediated cell adhesion to extracellular matrix proteins (8, 9). SHPS-1 thus functions as a docking protein to recruit and activate SHP-1 or SHP-2 at the cell membrane in response to extracellular stimuli. CD47 is a ligand for the extracellular region of SHPS-1 (10, 11). This protein, which was originally identified in association with $_{v}$ $_{3}$ integrin, is also a member of the Ig superfamily, possessing an Ig-V-like extracellular domain, five putative membrane-spanning segments, and a short cytoplasmic tail (12). Among hemopoietic cells, SHPS-1 is especially abundant in DCs, macrophages, and neutrophils, being barely detectable in T or B lymphocytes (11, 13–16). In contrast, CD47 is expressed in a variety of hemopoietic cells, including RBCs and T cells (12). Indeed, the interaction of CD47 on RBCs with SHPS-1 on macrophages is thought to prevent phagocytosis of the former cells by the latter through activation of SHP-1, which forms a complex with SHPS-1 (17–19). Similarly, SHPS-1, through its interaction with CD47, is also thought to play a negative role in the immune

*Department of Medicine and Clinical Science, Gunma University Graduate School of Medicine, Gunma, Japan; †Laboratory of Biosignal Sciences, Institute for Molecular and Cellular Regulation, Gunma University, Gunma, Japan; and ‡Department of Neurology, Gunma University Graduate School of Medicine, Gunma, Japan

Received for publication December 11, 2006. Accepted for publication May 8, 2007.

The costs of publication of this article were defrayed in part by the payment of page charges. This article must therefore be hereby marked *adveStTement* in accordance with 18 U.S.C. Section 1734 solely to indicate this fact.

[1] This work was supported by a Grant-in-Aid for Scientific Research on Priority Areas Cancer, a Grant-in-Aid for Scientific Research (B) and (C), a grant of Initiatives for Attractive Education in Graduate Schools, and a grant of the 21st Century Center of Excellence Program from the Ministry of Education, Culture, Sports, Science, and Technology of Japan.

[2] T.T., and Yu.K. contributed equally to this work.

[3] Address correspondence and reprint requests to Dr. Takashi Matozaki, Laboratory of Biosignal Sciences, Institute for Molecular and Cellular Regulation, Gunma University, 3-39-15 Showa-Machi, Maebashi, Gunma 371-8512, Japan; E-mail address: matozaki@showa.gunma-u.ac.jp or Dr. Yoriaki Kaneko, Department of Clinical Science, Gunma University, Graduate School of Medicine, 3-39-22 Showa-Machi, Maebashi, Gunma 371-8512, Japan; E-mail address: ykaneko@showa.gunma-u.ac.jp

[4] Abbreviations used in this paper: DC, dendritic cell; BMDC, DC derived from bone marrow; EAE, experimental autoimmune encephalomyelitis; LN, lymph node; MOG, myelin oligodendrocyte glycoprotein; ODN, oligodeoxynucleotide; SHP, Src homology 2 domain-containing protein tyrosine phosphatase; SHPS-1, SHP substrate-1; WT, wild type.

system (15). Ligation of SHPS-1 by CD47-Fc fusion proteins suppressed the phenotypic and functional maturation of immature DCs and inhibited cytokine production by mature DCs (15), suggesting that SHPS-1 (on DCs), through its interaction with CD47 (on T cells), prevents activation of DCs. In contrast, interaction of CD47 with SHPS-1 promotes the proliferation of T cells as well as contributes to the activation of Ag-specific CTL by DCs in vitro (16). Moreover, SHPS-1 also stimulates NO production by macrophages (20), suggesting that SHPS-1 would play a positive role in the immune system. These effects of SHPS-1 were demonstrated in vitro, however, with the physiological roles of SHPS-1 in the immune system remaining largely unknown. Furthermore, the possible role of SHPS-1 in autoimmune disease has not previously been investigated.

We previously generated mice that express a mutant version of SHPS-1 that lacks most of the cytoplasmic region (19, 21). This mutant protein does not undergo tyrosine phosphorylation or form a complex with SHP-1 or SHP-2. Furthermore, the cellular abundance of the mutant protein is markedly reduced compared with that of the full-length protein in wild-type (WT) cells (19, 21). With the use of these SHPS-1 mutant mice, we have now investigated the roles of SHPS-1 in the immune system and in the development of autoimmune disease.

Materials aOd Methods

Abs and reagents

Hybridoma cells producing the rat P84 mAb to SHPS-1 were provided by C. Lagenaur (University of Pittsburgh, Pittsburgh, PA); the mAb was purified from culture supernatants and conjugated to sulfo-NHS-LC biotin (sulfosuccinimidyl-6-(biotinamido) hexanoate; Pierce). Rabbit polyclonal Abs to SHPS-1 were obtained from ProSci. The mAbs to mouse CD16/32 (2.4G2) were prepared from the culture supernatants of hybridoma cells (provided by K. Okumura, Juntendo University, Tokyo, Japan). FITC-conjugated mAbs to mouse CD11c (HL3), CD4 (L3T4), or CD8 (Ly-2) as well as a biotin-conjugated mAb to mouse CD11c, biotin-conjugated rat IgG to trinitrophenol (isotype control), and PE- or FITC-conjugated streptavidin were from BD Pharmingen. FITC-conjugated mAbs to mouse NK1.1 (PK136) or B220 (RA3-6B2); biotin-conjugated mAbs to mouse MHC class I (28-14-8), MHC class II (M5/114.15.2), CD80 (16-10A1), CD86 (GL1), CD25 (PC61), or CD40 (3/23); and FITC-conjugated rat IgG to trinitrophenol (isotype control) were from eBioscience. Murine rIL-12 and rGM-CSF were from PeproTech, and murine rIFN- was from Pierce. RPMI 1640 medium (Sigma-Aldrich) was supplemented with 10% heat-inactivated FBS, 50 M 2-ME, 2 mM L-glutamine, 10 mM HEPES-NaOH (pH 7.4), penicillin (100 U/ml), streptomycin (100 g/ml), and 1 mM sodium pyruvate to yield complete medium.

Mice

Mice that express a mutant version of SHPS-1 that lacks most of the cytoplasmic region were described previously (19, 21) and were backcrossed onto the C57BL/6 background for five or six generations as well as for nine generations. Mice were bred and maintained at the Institute of Experimental Animal Research of Gunma University under specific pathogen-free conditions and were handled in accordance with the animal care guidelines of Gunma University.

Induction of experimental autoimmune encephalomyelitis (EAE) and histological analysis

EAE was induced in 6- to 12-wk-old male C57BL/6 WT or SHPS-1 mutant mice by s.c. injection (into the base of the tail and rump) with a total of 100 g of a peptide derived from mouse (rat) myelin oligodendrocyte glycoprotein (MOG (35–55)) (MEVGWYRSPFSRVVHLYRNGK) in CFA containing 400 g of heat-inactivated *Mycobacterium tuberculosis* (Difco) (22, 23). Pertussis toxin (200 ng) (List Biological Laboratories) was also injected i.p. on days 0 and 2. Animals were observed daily for clinical signs of EAE for up to 35 days after immunization, and neurological effects were quantified on an arbitrary clinical scale: 0, no disease; 1, limp tail; 2, hindlimb weakness; 3, total hindlimb paralysis; 4, hind- and forelimb paralysis; and 5, death. The mean clinical score was calculated by averaging the scores of all mice in each group, including animals that did not develop EAE. For histological analysis, mice were perfused transcardially with 4% paraformaldehyde in PBS, after which the spinal cord was removed, embedded in paraffin, sectioned, and stained with Mayer's H&E.

Cell proliferation and cytokine production in spleen or LN cells

The spleen or LNs were removed from mice 10 days after immunization with MOG. The tissue was gently ground with autoclaved frosted glass slides in PBS, and RBCs were hypotonically lysed by incubation of the resulting cell suspension with Gey's solution. The remaining lymphocytes from LNs were washed twice with PBS, and the cells (5 10^5 per well) were then cultured with various concentrations of MOG (35–55) for 72 h under an atmosphere of 5% CO_2 at 37°C in 96-well, round-bottom microplates (Falcon). The cells were exposed to 1 Ci of [^{3}H]TdR for the final 14 h of the incubation and were then harvested on glass fiber filters with the use of an automated sample harvester (PerkinElmer). The incorporated radioactivity was measured with a scintillation spectrometer (PerkinElmer). For measurement of cytokine production from spleen cells, the culture supernatants obtained after incubation of the cells for 72 h with the MOG peptide were collected and assayed for IFN- (BD Pharmingen), IL-2 (BD Pharmingen), IL-10 (BD Pharmingen), and IL-17 (R&D Systems) with the use of ELISA kits.

Assay for serum Abs to MOG

The relative titers of Abs to MOG in serum samples were measured, as described previously (24). Serum samples were obtained from blood of MOG-primed WT and SHPS-1 mutant mice 40 days after immunization. A 96-well flat-bottom plate was coated with 5 g/ml MOG (35–55) peptide at 4°C overnight. After washing the wells with PBS containing 0.05% Tween 20, the wells were blocked with 0.25% skim milk in PBS for 1 h at 37°C. After washing, diluted serum samples (diluted 1/30 or 1/300 in PBS) were added and incubated for 2 h at 37°C. Thereafter, HRP-conjugated goat polyclonal Abs to mouse IgG (Zymed Laboratories), IgG1, and IgG2a (Bethyl Laboratories) were added (concentration 1/4,000 or 1/40,000 in PBS). Plates were incubated for 2 h at 37°C. Tetramethylbenzidine substrate reagent set (BD Pharmingen) was used to develop the plates, and the reaction was stopped with stop solution (BD Pharmingen), and read at 450 nm.

Preparation of splenic DCs and T cells

Immature or mature splenic CD11c DCs were prepared from collagenase-digested spleen tissue, as described (25, 26), with minor modifications. In brief, splenocytes were released by homogenization of the spleen and subsequent exposure (with repeated passage through the tip of a pipette) of the tissue for 30 min at room temperature to collagenase (WAKO) at 400 U/ml in the presence of 5 mM EDTA. The undigested fibrous material was removed by filtration through a nylon mesh, and RBCs in the filtrate were lysed with Gey's solution. The remaining cells were washed twice with PBS, suspended in 2 ml of Ca^2 - and Mg^2 -free HBSS (Invitrogen Life Technologies) containing 17% Optiprep (Nycomed), and overlaid consecutively with 2 ml of 12% Optiprep in 10 mM HEPES-NaOH (pH 7.4), 0.88% NaCl, 1 mM EDTA, and 0.5% BSA, and with 2 ml of Ca^2 - and Mg^2 -free HBSS. The resulting gradient was centrifuged at 700 *g* for 15 min at 20°C, after which cells at the interface of the top two layers were collected and washed twice with PBS. Immature CD11c DCs were then isolated from the washed cells with the use of magnetic beads coated with a mAb to CD11c and a MACS column (Miltenyi Biotec). For isolation of mature DCs, the washed cells were suspended in RPMI 1640 complete medium and cultured for 2 h in a plastic dish; the nonadherent cells were then removed, and the remaining adherent cells were incubated for an additional 18 h. The newly nonadherent cells were then harvested, and mature CD11c DCs were isolated from this fraction with the use of magnetic beads coated with a mAb to mouse CD11c. Purified DCs were routinely 95% CD11c as determined by flow cytometry. For preparation of splenic CD4 or CD8 T cells (27, 28), the spleen was gently ground with autoclaved frosted glass slides in PBS, and the released cells were exposed to Gey's solution, washed twice with PBS, and filtered through nylon wool. Cells in the filtrate were then subjected to purification with the use of magnetic beads coated with mAbs to mouse CD4 or CD8 and a MACS column (Miltenyi Biotec). The purity of the isolated CD4 or CD8 T cells was 95% as determined by flow cytometry.

Flow cytometric and immunoblot analysis of DCs

For examination of the surface expression of SHPS-1 on DCs, immature splenic CD11c DCs (1 10^6) were first incubated with a mAb to mouse CD16/32 (1 g/ml) to avoid nonspecific binding of labeled mAbs to FcR . The cells were then washed and incubated consecutively with a biotin-conjugated mAb to SHPS-1 (1 g/ml) and streptavidin FITC (0.2 g/ml)

before flow cytometric analysis with a FACSCalibur instrument and CellQuest software (BD Biosciences). For immunoblot analysis, immature splenic CD11c DCs were homogenized on ice in a solution containing 20 mM Tris-HCl (pH 7.6), 140 mM NaCl, 1 mM EDTA, 1% Nonidet P-40, 1 mM PMSF, aprotinin (10 g/ml), and 1 mM sodium vanadate. The lysates were centrifuged at 10,000 *g* for 15 min at 4°C, and the resulting supernatants were subjected to immunoblot analysis (18).

MLRs

Immature CD11c DCs prepared from WT or SHPS-1 mutant mice were exposed to -radiation (30 Gy) and then plated in 96-well, round-bottom microplates. CD4 or CD8 T cells were purified from BALB/c splenocytes by magnetic cell separation. Purified responder T cells (1 10^5 per well) were then cultured with the stimulator cells for 72 h, with [^{3}H]TdR (1 Ci per well) being added for the final 12 h. Cells were harvested on glass fiber filters, and the incorporated radioactivity was measured. The culture supernatants were also assayed for IFN- , IL-2, and IL-10. In another set of experiments, irradiated immature CD11c DCs from BALB/c mice were incubated with CD4 or CD8 T cells from WT or SHPS-1 mutant mice, and proliferation of the responder cells was determined.

Proliferation of T cells from OT-II mice

For assay of the proliferation of OT-II CD4 T cells in vitro (29), 8- to 12-wk-old male WT or SHPS-1 mutant mice were injected i.v. with 3 mg of OVA (Calbiochem) or vehicle. Twelve hours after the injection, immature CD11c DCs were purified from the spleen and cultured for 72 h at various densities with OT-II CD4 T cells (1 10^5 per well) in 96-well, round-bottom microplates; the final 12 h of culture were performed in the additional presence of [^{3}H]TdR (1 Ci per well), and the cell-associated radioactivity was subsequently measured with a scintillation spectrometer.

Assay of TLR- or IL-12-induced cytokine production

For the preparation of DCs derived from bone marrow (BMDCs), bone marrow cells were isolated from the femur and tibia of WT or SHPS-1 mutant mice with the use of a syringe fitted with a 23-gauge needle (30, 31). The cells (1 10^6/ml) were seeded onto a 24-well culture plate in RPMI 1640 complete medium supplemented with GM-CSF (10 ng/ml), and the culture medium was changed every 2 days to remove granulocytes. After culture for 6–7 days, loosely adherent and clustered cells were collected as immature BMDCs. For assay of cytokine production by BMDCs (30), the cells were stimulated for 20 h with LPS (Sigma-Aldrich) at 1 g/ml or 1 M phosphorothioate oligodeoxynucleotide (ODN) with a CpG motif (CpG ODN) 1826 (5 -TCCATGACGTTCCTGACGTT-3) (Japan Bio Services) in the absence or presence of IFN- (10 ng/ml). Culture supernatants were then assayed for IL-12p70 (R&D Systems) as well as TNF- and IL-6 (BD Pharmingen) with ELISA kits. In other experiments, mature splenic CD11c DCs (1 10^5 per well of 96-well, round-bottom microplates) were cultured for 72 h in RPMI 1640 complete medium with various concentrations of IL-12. Culture supernatants were than assayed for IFN- with an ELISA kit.

Adoptive transfer

Adoptive transfer of T cells from WT mice was performed, as described previously (22). In brief, WT mice were immunized with 100 g of MOG (35–55), and, after 10 days, draining LNs were harvested for isolation of lymphocytes. The cells were cultured with MOG (35–55) (10 g/ml) and IL-12 (5 ng/ml) for 4 days, washed with PBS, and resuspended in PBS for transfer. WT or SHPS-1 mutant mice were injected i.v. with the lymphocytes (1 10^7) as well as with 200 ng of pertussis toxin (both immediately and 2 days after cell transfer). The animals were observed daily, and neurological effects were quantified, as described above.

4tatistical analysis

Data are presented as means SE and were analyzed by Student's *t* test with the use of Stat View 5.0 software (SAS Institute). A *p* value of 0.05 was considered statistically significant.

Results

Resistance of 4) P4-1 mutant mice to EAE

We first examined the susceptibility of the SHPS-1 mutant mice to EAE, an animal model of multiple sclerosis. EAE was induced by immunizing mice; those were backcrossed onto the C57BL/6 background for five or six generations, with MOG (35–55) (32, 33). Fourteen of 15 (93%) WT mice developed typical EAE 14

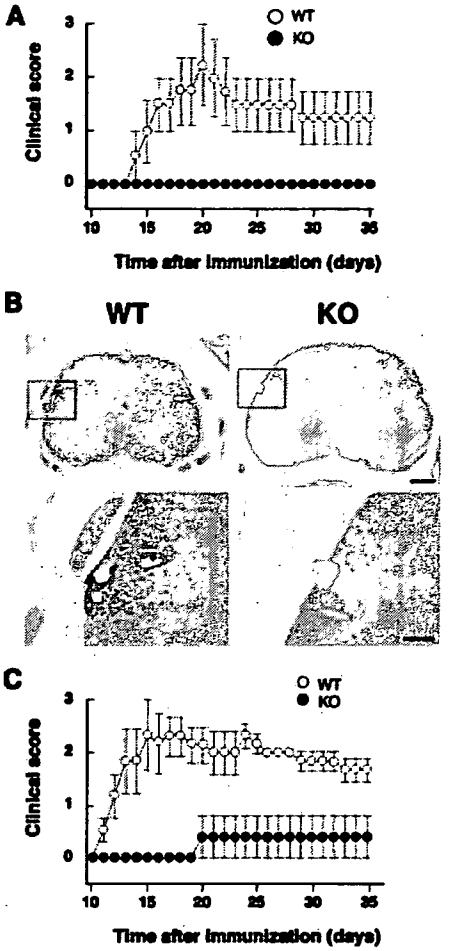

FIGURE 1. Resistance of SHPS-1 mutant mice to EAE. *A*, Time course of the clinical score of WT and SHPS-1 mutant (knockout (KO)) mice; those were backcrossed on the C57BL/6 background for five to six generations and immunized with MOG (35–55), as described in *Materials and Methods*. Data are means SE (*n* 4) and are representative of four independent experiments. *B*, Histopathology of the spinal cord of WT and SHPS-1 mutant (KO) mice 20 days after immunization with MOG (35–55). The boxed regions of the *upper panels* are shown in the *lower panels*. H&E staining shows marked infiltration of mononuclear cells around the blood vessels in WT mice, but not in the mutant mice. Scale bars: 200 m (*upper panels*) and 50 m (*lower panels*). *C*, Time course of the clinical score of WT and SHPS-1 mutant (KO) mice; those were backcrossed on the C57BL/6 background for nine generations and immunized with MOG (35–55). Data are means SE (*n* 6) and are representative of three independent experiments.

days after immunization with MOG (35–55) and pertussis toxin. In marked contrast, none of the 15 similarly immunized SHPS-1 mutant mice developed EAE. The time course and severity of EAE in WT mice compared with data for SHPS-1 mutant mice in a typical experiment are shown in Fig. 1*A*. Histological analysis of the spinal cord revealed pronounced infiltration of mononuclear cells around blood vessels 20 days after immunization in WT mice, whereas no such inflammatory response was observed in SHPS-1 mutant mice (Fig. 1*B*). Furthermore, we also examined the susceptibility of the SHPS-1 mutant mice to EAE by the use of mice; those were backcrossed onto the C57BL/6 background for nine generations. We found that such SHPS-1 mutant mice were also resistant to EAE, compared with WT mice (Fig. 1*C*). Thirteen of 14 (93%) WT mice developed typical EAE with MOG (35–55) and pertussis toxin. In contrast, only 4 of the 13 SHPS-1 mutant

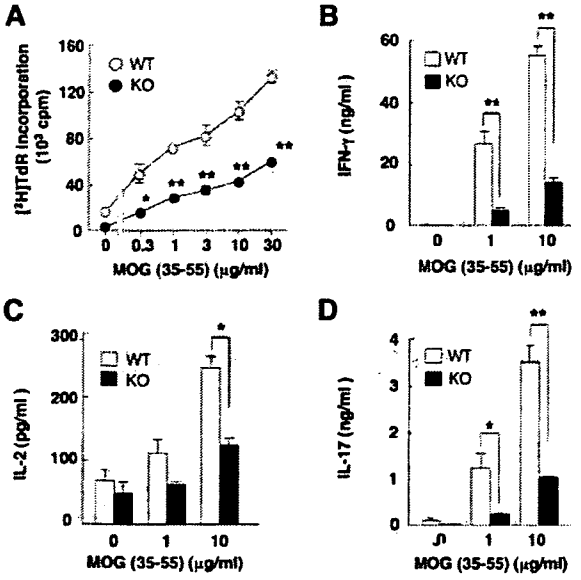

FIGURE 2. Impaired MOG (35–55)-induced proliferation of, and production of cytokines by, T cells from immunized SHPS-1 mutant mice. Lymphocytes (*A*) or splenocytes (*B–D*) prepared from WT or SHPS-1 mutant (knockout (KO)) mice 10 days after immunization with MOG (35–55) were assayed for cell proliferation (*A*) and production of IFN- (*B*), IL-2 (*C*), or IL-17 (*D*) after exposure to various concentrations of MOG (35–55). Data are means SE of triplicate determinations and are representative of three independent experiments. , p 0.05; , p 0.01 vs WT mice or for the indicated comparisons (Student's t test).

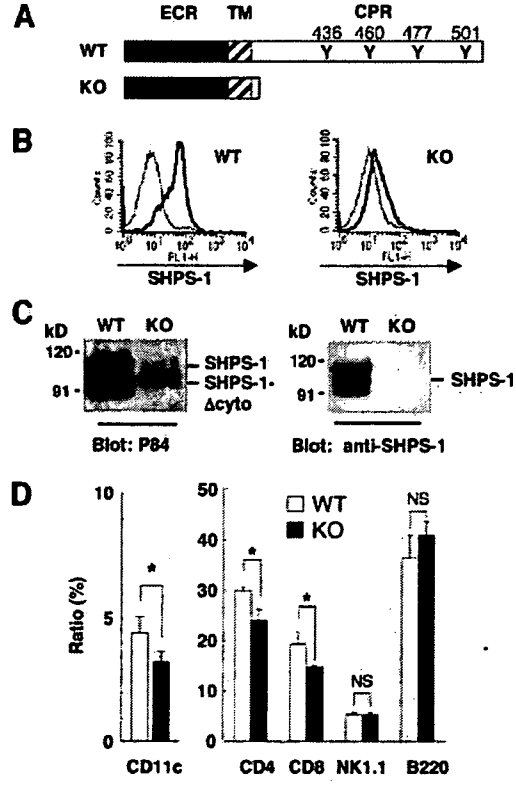

FIGURE 3. Flow cytometric and immunoblot analysis of SHPS-1 expression in CD11c DCs and reduced numbers of CD11c DCs as well as CD4 or CD8 T cells in SHPS-1 mutant mice. *A*, Schematic representations of WT and mutant (knockout (KO)) forms of mouse SHPS-1. ECR, extracellular region; TM, transmembrane region; CPR, cytoplasmic region; Four putative tyrosine (Y) phosphorylation sites in the cytoplasmic region are indicated. *B*, Immature CD11c DCs prepared from the spleen of WT or SHPS-1 mutant (KO) mice at 6 wk of age were stained with biotinylated mAb P84 (thick trace) or an isotype control mAb (thin trace) and then with FITC-conjugated streptavidin. The expression of SHPS-1 was then examined by flow cytometry. *C*, Lysates of splenic immature CD11c DCs derived from WT or SHPS-1 mutant (KO) mice at 6 wk of age were subjected to immunoblot analysis with a mAb to the extracellular region of SHPS-1 (P84) or with polyclonal Abs to the cytoplasmic region of SHPS-1 (anti-SHPS-1), as indicated. The positions of WT (SHPS-1) and mutant (SHPS-1- cyto) forms of SHPS-1 are indicated. *D*, The percentages of CD11c DCs, CD4 T cells, CD8 T cells, NK1.1 cells, and B220 B cells in the spleen of WT or SHPS-1 mutant (KO) mice at 6 wk of age were determined by flow cytometry. Data are means SE of values from six mice of each genotype. , p 0.05 for the indicated comparisons (Student's t test).

mice developed EAE, and the clinical score for such SHPS-1 mutant mice was lower than that for WT mice. We therefore next compared the MOG-specific proliferative response of and cytokine production by T cells derived from MOG-primed animals. The cell proliferation and production of IFN- in response to MOG were markedly reduced in lymphocytes derived from MOG-primed SHPS-1 mutant mice compared with the responses of WT cells (Fig. 2, *A* and *B*). The production of IL-2 in response to MOG was also reduced in splenic lymphocytes derived from MOG-primed SHPS-1 mutant mice compared with the responses of WT cells (Fig. 2*C*). In contrast, the production of IL-10 in response to MOG was minimal in splenic lymphocytes derived from MOG-primed WT or SHPS-1 mutant mice (data not shown). The production of IL-17 by MOG-primed Th17 cells was recently shown to be essential for development of EAE (34–36). The MOG-induced production of IL-17 was also greatly reduced in splenic lymphocytes derived from MOG-primed SHPS-1 mice compared with that apparent with WT cells (Fig. 2*D*). We also examined the relative titers of Abs to MOG in serum samples from MOG-primed WT and SHPS-1 mutant mice 40 days after immunization. However, no marked difference was observed in IgG, IgG1, and IgG2a titers between WT and mutant mice (data not shown).

Reduced numbers of CD11c DCs as well as CD4 or CD8 T cells in 4) P4-1 mutant mice

Induction of EAE requires T cell responses that are initiated by priming of naive CD4 T cells by DCs. SHPS-1 mutant mice express a mutant version of SHPS-1 that lacks most of the cytoplasmic region (Fig. 3*A*) (19, 21). Flow cytometry and immunoblot analysis with the P84 mAb to the extracellular region of SHPS-1 confirmed that SHPS-1 is expressed on CD11c DCs (Fig. 3, *B* and *C*). The abundance of SHPS-1 was substantially reduced in CD11c DCs from the spleen of SHPS-1 mutant mice compared with that apparent for WT cells (Fig. 3, *B* and *C*). In addition, immunoblot analysis with polyclonal Abs specific for the cytoplasmic region of SHPS-1 yielded no signal with splenic DCs from the homozygous mutant mice (Fig. 3*C*). These results suggested that the minimal susceptibility of SHPS-1 mutant mice to EAE may be attributable to a functional defect of DCs in priming of naive CD4 T cells. We therefore characterized the functions of DCs in SHPS-1 mutant mice. We first showed that the number of CD11c DCs in the spleen was reduced in the mutant animals (Fig. 3*D*), although the total number of splenic cells was not altered (data not shown) (19). Small decreases in the numbers of CD4 or CD8 T cells were also apparent in the spleen of SHPS-1 mutant mice, whereas the numbers of B220 B cells or NK1.1 NK cells (or NK T cells) did not differ between the mutant and WT

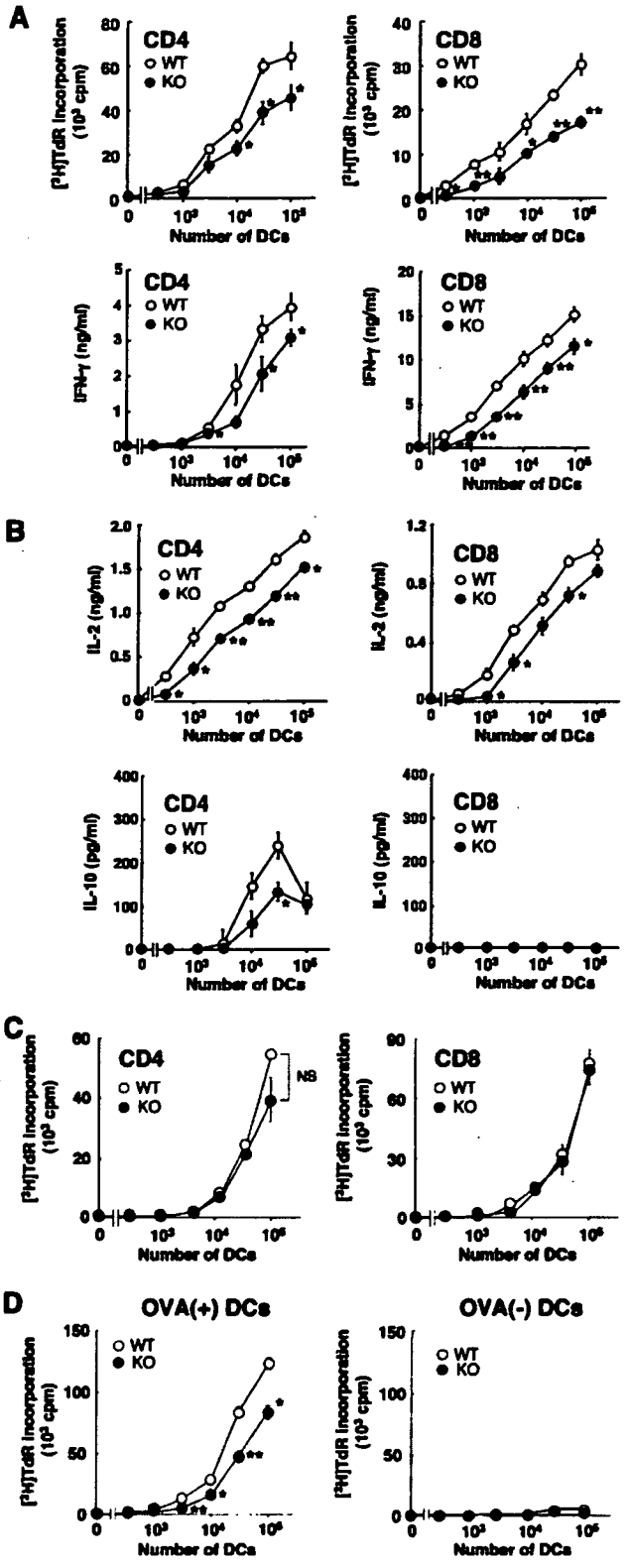

FIGURE 4. Impaired function of CD11c DCs from SHPS-1 mutant mice in an allogenic MLR and in priming of OVA-specific CD4 T cells. *A*, Cell proliferation (*upper panels*) and IFN- production (*lower panels*) were determined in MLRs with various numbers of irradiated immature CD11c DCs of WT or SHPS-1 mutant (knockout (KO)) mice and with splenic CD4 or CD8 T cells (1 10^5) from BALB/c mice. *B*, The production of IL-2 or IL-10 was determined in MLRs with various numbers of irradiated immature CD11c DCs of WT or SHPS-1 mutant (KO) mice and with splenic CD4 or CD8 T cells (1 10^5) from BALB/c mice. *C*, Cell proliferation in MLRs with various numbers of irradiated immature CD11c DCs of BALB/c mice and with splenic CD4 or CD8 T cells (1 10^5) from WT or SHPS-1 mutant mice. *D*, Immature CD11c DCs derived from the spleen of WT or SHPS-1 mutant (KO) mice injected with OVA (*left panel*) or vehicle (*right panel*) were cultured at various densities with CD4 T cells (1 10^5) from OT-II mice, after which cell proliferation was determined. Data in all panels are means SE of values from triplicate determinations and are representative of three separate experiments. , p 0.05; , p 0.01 vs WT (Student's t test).

animals (Fig. 3*D*). These data suggested that SHPS-1 regulates the number of CD11c DCs as well as those of T cells in the spleen.

Reduced abilities of DCs from 4) P4-1 mutant mice to stimulate an allogenic MLR and the proliferation of Ag-specific CD4 T cells

We next examined the ability of DCs from SHPS-1 mutant mice to stimulate alloreactive CD4 or CD8 T cells. In MLRs with CD11c DCs isolated from SHPS-1 mutant mice, the proliferation of CD4 or CD8 T cells from BALB/c mice was markedly reduced, compared with that apparent with DCs from WT mice (Fig. 4*A*). Consistent with this finding, the production of IFN- was also reduced on incubation of the CD4 or CD8 T cells with DCs from SHPS-1 mutant mice (Fig. 4*A*). In addition, the production of IL-2 was reduced on incubation of the CD4 or CD8 T cells with DCs from SHPS-1 mutant mice (Fig. 4*B*). The production of IL-10 was slightly reduced on incubation of the CD4 T cells with DCs from SHPS-1 mutant mice, whereas it was not detected on incubation of the CD8 cells with DCs from either WT or SHPS-1 mutant mice (Fig. 4*B*). In contrast, the proliferation of CD4 or CD8 T cells from SHPS-1 mutant mice was similar to that of the corresponding WT cells on incubation with DCs from BALB/c mice (Fig. 4*C*). These results suggested that DCs, but not CD4 or CD8 T cells, of SHPS-1 mutant mice are functionally defective in an allogenic MLR.

To characterize further the dysfunction of DCs in SHPS-1 mutant mice, we examined the proliferation of OVA-specific CD4 T cells (prepared from OT-II transgenic mice (37)) in response to culture with OVA-pulsed CD11c DCs. The proliferation of OVA-specific CD4 T cells cultured with DCs from SHPS-1 mutant mice was markedly impaired compared with that of those cultured with DCs from WT mice (Fig. 4*D*), suggesting that priming of Ag-specific T cells by DCs is indeed defective in SHPS-1 mutant mice.

Impaired TLR-dependent cytokine production and IL-12-induced IFN- release in DCs from 4) P4-1 mutant mice

We therefore next examined what specific activity of DCs might be impaired in SHPS-1 mutant mice. For priming of naive T cells, DCs first capture exogenous Ags and then migrate from peripheral tissues to draining LNs, where they encounter naive T cells and present MHC-peptide complexes (1, 2). During this process, DCs also mature and express multiple costimulatory molecules; such as CD80, CD86, and CD40, on their surface. They also secrete IL-12, a key cytokine that promotes the production of IFN- not only by Th1 cells, but also by DCs themselves. However, neither the migratory response of, nor the uptake of FITC-labeled BSA by, BMDCs differed substantially between SHPS-1 mutant and WT mice (Fig. 5, *A* and *B*). In addition, the up-regulation of surface molecules, including MHC class I and II as well as CD80, CD86, and CD40, on splenic CD11c DCs during their maturation also appeared similar for WT and SHPS-1 mutant mice (Fig. 5*C*).

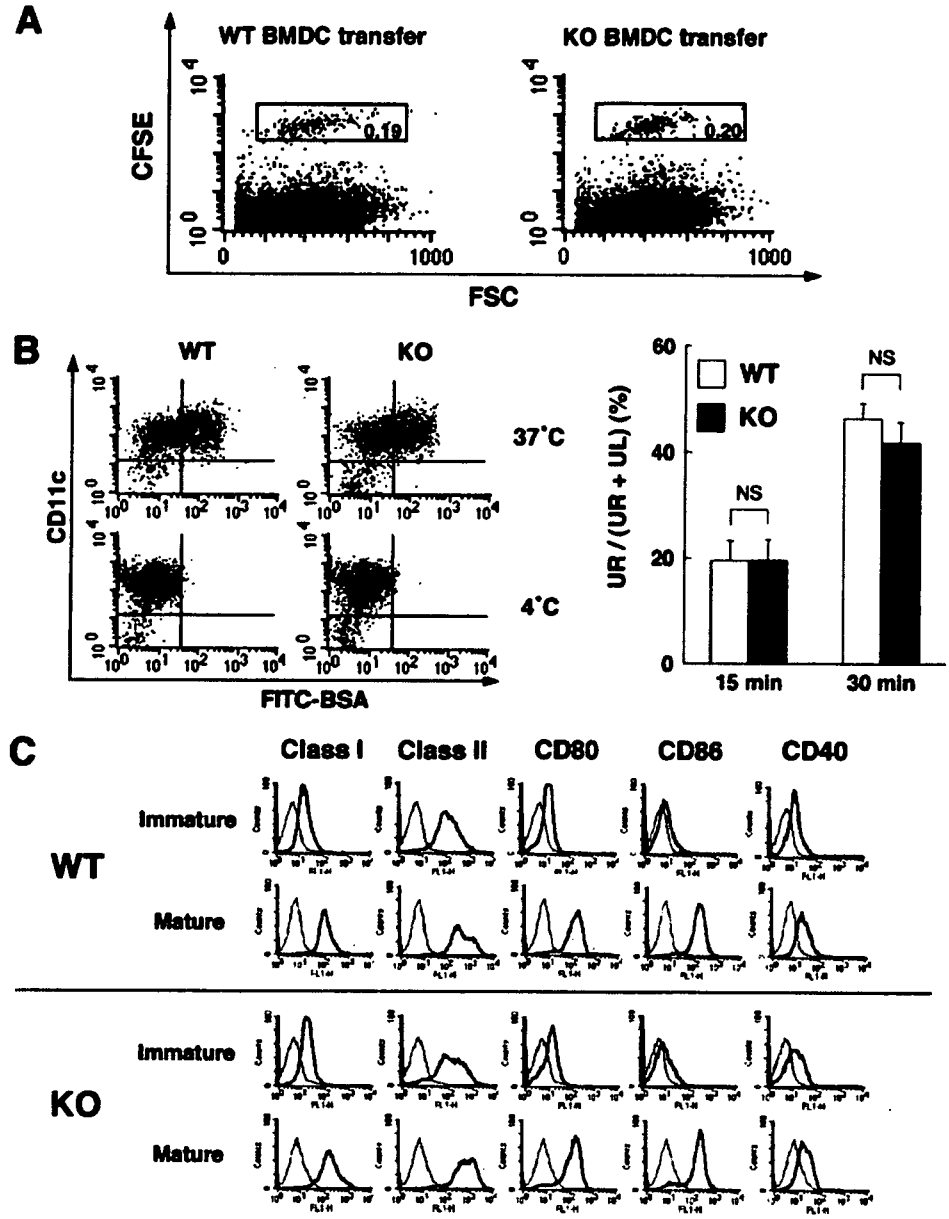

FIGURE 5. Migration, Ag uptake, and differentiation in DCs from WT and SHPS-1 mutant mice. *A*, BMDCs derived from WT or SHPS-1 mutant (knockout (KO)) mice were labeled with 10 M CFSE for 10 min at 37°C in RPMI 1640, as described (31), washed three times, and then resuspended (5 10^6 cells in 40 l) in PBS and injected into a hind footpad of WT mice. Three days after injection, lymphocytes were isolated from the draining LNs and subjected to flow cytometric analysis for determination of the percentage of cells labeled with CFSE (gated area). Data are from a representative experiment. The mean SE values for the percentage of migrating cells were 0.17 0.01 and 0.11 0.05 for WT and SHPS-1 mutant mice, respectively (n 3, p 0.05). FSC, forward scatter. *B*, BMDCs from WT or SHPS-1 mutant (KO) mice were incubated with FITC-BSA (5 g/ml) (Sigma-Aldrich) at 37°C or 4°C (control) for 15 or 30 min, washed, and then stained with biotin-conjugated Abs to mouse CD11c and PE-conjugated streptavidin. FITC-BSA uptake by CD11c DCs was then monitored by flow cytometry. Data shown in the *left panels* were obtained with cells incubated for 30 min and are representative of three separate experiments. The uptake of FITC-BSA by CD11c DCs at 15 or 30 min and 37°C was also determined as the percentage of CD11c DCs that had incorporated FITC-BSA (cells in the *upper right* (UR) *quadrant*) among total CD11c DCs (sum of the cells in the *upper right* and *upper left* (UL) *quadrants*), as shown in the *right panel*; data are means SE of values from three separate experiments. *C*, Immature or mature CD11c DCs prepared from the spleen of WT or SHPS-1 mutant (KO) mice were incubated first with biotin-conjugated mAbs to mouse MHC class I, MHC class II, CD80, CD86, or CD40 (thick traces), or with an isotype control mAb (thin traces) and then with FITC-conjugated streptavidin. They were then analyzed by flow cytometry. Data are representative of three separate experiments.

We then evaluated the TLR-dependent production of cytokines by BMDCs. The production of 70-kDa heterodimeric IL-12 (IL-12p70) in response to either LPS or CpG ODN was slightly impaired in BMDCs from SHPS-1 mutant mice (Fig. 6*A*). Moreover, the production of TNF- and IL-6 in response to either LPS or CpG ODN was markedly impaired in BMDCs from the mutant animals (Fig. 6*A*). The IL-12-induced production of IFN- by DCs is important for DC functions (25, 26, 38). We found that the IL-12-induced production of IFN- in splenic CD11c DCs from SHPS-1 mutant mice was greatly reduced compared with that

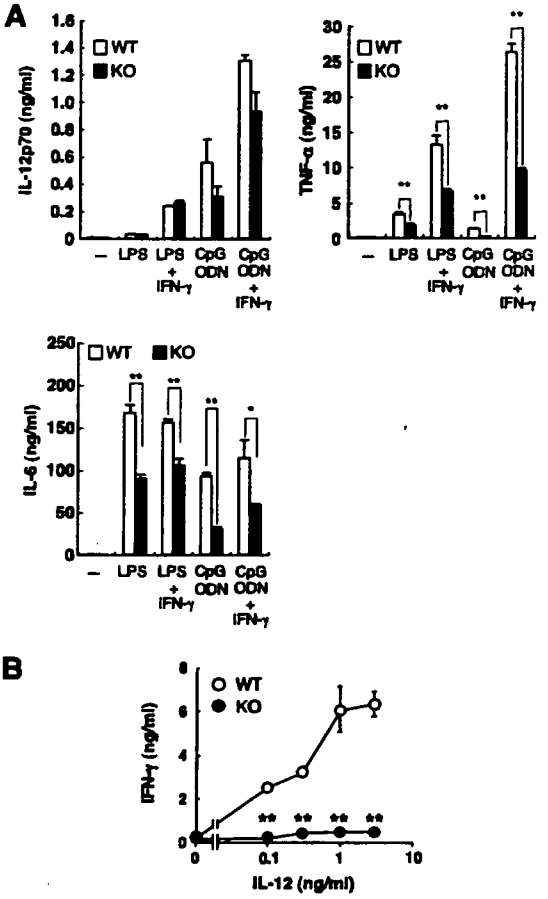

FIGURE 6. Impaired TLR-dependent cytokine production and IL-12-induced IFN- production in DCs from SHPS-1 mutant mice. *A*, BMDCs from WT or SHPS-1 mutant (knockout (KO)) mice were stimulated with LPS (1 g/ml) or CpG ODN (1 M) in the absence or presence of IFN- (10 ng/ml) for 20 h, after which the levels of the indicated cytokines in culture supernatants were determined. *B*, Mature CD11c DCs from the spleen of WT or SHPS-1 mutant (KO) mice were cultured with various concentrations of IL-12 for 72 h, after which the concentration of IFN- in culture supernatants was determined. All data are means SE of values from triplicate determinations and are representative of three separate experiments. ,p 0.05; ,p 0.01 vs WT or for the indicated comparisons (Student's t test).

apparent with WT cells (Fig. 6*B*). These data thus suggested that SHPS-1 is essential for TLR-dependent cytokine production as well as the IL-12-induced production of IFN- by DCs.

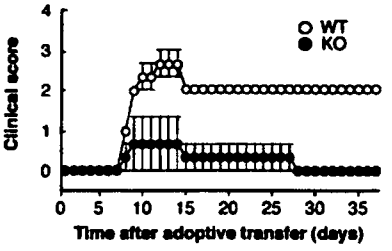

FIGURE 7. Impaired induction of EAE in SHPS-1 mutant mice by adoptive transfer of T cells from WT donor mice. Time course of the clinical score of WT or SHPS-1 mutant (knockout (KO)) mice injected with MOG-specific lymphocytes prepared from WT mice, as described in *Materials and Methods*. Data are means SE (n 3) and are representative of three separate experiments.

Impaired induction of EAE in 4) P4-1 mutant mice by adoptive transfer of T cells from WT donor mice

Given that development of EAE was blocked in SHPS-1 mutant mice, it was possible that these animals have a defect in the effector phase of this condition as well as in the priming of T cells by DCs. We therefore performed adoptive transfer of T cells derived from MOG-primed WT mice into either WT or SHPS-1 mutant mice. Adoptive transfer of MOG-primed T cells from WT donor mice induced EAE in WT mice, but this effect was markedly diminished in SHPS-1 mutant mice (Fig. 7).

DiscussioO

We have shown in this study that SHPS-1 mutant mice are resistant to EAE. Moreover, the MOG-induced proliferation of and production of IFN- as well as of IL-2 by T cells from immunized SHPS-1 mutant mice were markedly reduced compared with those apparent for WT cells. It was recently shown that IL-17 produced by Th17 cells in response to TGF- , IL-6, or IL-23 is essential for development of EAE (34, 35). Indeed, IL-17-deficient mice also manifest minimal susceptibility to EAE (36). We found that the MOG-induced production of IL-17 by T cells from immunized SHPS-1 mutant mice was reduced compared with that apparent for WT cells. Induction of EAE requires T cell responses that are initiated by priming of naive CD4 T cells by DCs. Given that SHPS-1 is expressed selectively in DCs, these results suggest that the resistance of SHPS-1 mutant mice to EAE is attributable to a defect in priming of CD4 T cells by DCs.

This notion was further supported by the observations that, in an allogenic MLR with CD11c DCs from SHPS-1 mutant mice, the proliferation of and production of IFN- by CD4 or CD8 T cells from BALB/c mice were markedly reduced, compared with those apparent with DCs from WT mice. Furthermore, the proliferation of OVA-specific CD4 T cells primed with DCs from SHPS-1 mutant mice was markedly impaired compared with that of those primed with DCs from WT mice. These results thus suggest that priming of either allogenic or Ag-specific T cells by DCs from SHPS-1 mutant mice is indeed defective. The interaction of SHPS-1 on macrophages with CD47 on RBCs prevents phagocytosis of RBCs by macrophages in a manner dependent on SHP-1, which binds the cytoplasmic region of SHPS-1 (17–19, 39). Moreover, SHPS-1 on DCs, through its interaction with CD47 on T cells, prevents activation of DCs (15), suggesting that SHPS-1 negatively regulates functions of macrophages and DCs. However, our present results demonstrate a positive regulatory role for SHPS-1 in efficient priming by DCs of naive T cells both in vivo and in vitro.

We investigated what specific function of DCs is actually impaired in SHPS-1 mutant mice. The abilities to migrate and to take up Ag were not markedly impaired in BMDCs from SHPS-1 mutant mice. In contrast, the TLR-dependent production of cytokines, including TNF- and IL-6, was defective in BMDCs from the mutant animals. Moreover, the IL-12-stimulated production of IFN- by DCs from SHPS-1 mutant mice was greatly impaired compared with that in WT cells. This effect of IL-12 is thought to be important for priming and activation of naive T cells by DCs (25, 26, 38). The impairment in priming of T cells by DCs of SHPS-1 mutant mice may thus be attributable, at least in part, to the defects in IL-12-induced production of IFN- and in TLR-dependent cytokine production in DCs. The molecular mechanism by which SHPS-1 positively regulates the effect of IL-12 on IFN- production by DCs remains unknown. The JAK2-STAT4 signaling pathway and the p38 isoform of MAPK are implicated in this effect of IL-12 (26, 40). Given that SHP-2 positively regulates

activation of the JAK-STAT pathway and MAPK signaling (41) and complex formation of SHPS-1 with SHP-2 is specifically defective in the SHPS-1 mutant mice, it is possible that the SHPS-1–SHP-2 complex positively regulates the action of IL-12 as well as that of other related cytokines that activate the JAK-STAT pathway and p38 MAPK in DCs.

Interaction of SHPS-1 (on DCs) with CD47 (on T cells) may contribute to the activation of T cells in a manner functionally similar to that apparent for costimulatory molecules on DCs such as B7 (which interacts with CD28 on T cells) and OX40 ligand (which interacts with OX40 on T cells). Mice deficient in either B7 or OX40 ligand indeed manifest a reduced susceptibility to EAE (22, 42). In addition, it was recently shown that delayed-type hypersensitivity to 2,4-dinitro-1-fluorobenzene, which is also thought to be mediated by Th1 cells, is markedly diminished in CD47-deficient mice (43). Conversely, we found that such delayed-type hypersensitivity is greatly reduced in extent in SHPS-1 mutant mice (44). Moreover, ligation of CD47 on T cells is thought to generate costimulatory signals for T cell activation (45). Together with the present results, these observations suggest a notion that interaction of SHPS-1 (on DCs) with its ligand CD47 (on T cells) is essential for priming of T cells by DCs.

We showed that induction of EAE by adoptive transfer of MOG-specific T cells from WT donor mice was impaired in SHPS-1 mutant mice, suggesting that these animals have a defect in the effector phase of EAE development as well as in the priming of T cells by DCs. It is possible that the production of chemokines or cytokines from various cell types, including macrophages and neutrophils, in the effector phase of EAE is impaired in SHPS-1 mutant mice. Secondary priming of T cells by APCs surrounding blood vessels of the CNS is also important for the development of EAE (46, 47). The reduced effect of adoptive transfer of MOG-specific T cells in SHPS-1 mutant mice may thus be attributable to a defect in secondary priming of the transferred T cells by host DCs.

Overall, our present study clearly indicates that SHPS-1 positively regulates the priming of T cells by DCs, and hence, that this protein is essential for the development of EAE. We found that SHPS-1 is required for multiple functions of DCs, including the IL-12-induced production of IFN- as well as the TLR-dependent production of cytokines by these cells. Our results also implicate SHPS-1 on DCs in the activation of T cells (presumably through interaction with CD47 on T cells) in a manner functionally similar to that apparent for other costimulatory molecules on DCs. We have recently shown that SHPS-1 mutant mice also manifest minimal susceptibility to collagen-induced arthritis, an animal model of rheumatoid arthritis (C. Okuzawa, Y. Kaneko, and T. Matozaki, unpublished observation), suggesting that SHPS-1 may contribute to development of various inflammatory autoimmune diseases. Given that the function of SHPS-1 is susceptible to regulation by ligands such as Abs, this protein is a potential therapeutic target for inflammatory autoimmune diseases in general.

AckOowledgmeOts

We thank C. F. Lagenaur for the mAb to SHPS-1; K. Okumura for the mAbs to CD16/32; D. Kamimura, M. Murakami, and T. Hirano for OT-II mice; S. Koyasu and T. Takai for suggestions and discussion; as well as A. Morita, Y. Niwayama, Y. Hayashi, and R. Koitabashi for technical assistance.

Disclosures

The authors have no financial conflict of interest.

RefereOces

1. Banchereau, J., and R. M. Steinman. 1998. Dendritic cells and the control of immunity. *NatuSe* 392: 245–252.
2. Moser, M., and K. M. Murphy. 2000. Dendritic cell regulation of T_H1-T_H2 development. *Nat. Immunol.* 1: 199–205.
3. Crow, M. K. 2006. Modification of accessory molecule signaling. *4pSinHŁS 4emin. Immunopathol.* 27: 409–424.
4. Fujioka, Y., T. Matozaki, T. Noguchi, A. Iwamatsu, T. Yamao, N. Takahashi, M. Tsuda, T. Takada, and M. Kasuga. 1996. A novel membrane glycoprotein, SHPS-1, that binds the SH2-domain-containing protein tyrosine phosphatase SHP-2 in response to mitogens and cell adhesion. *Mol. Cell. Biol.* 16: 6887–6899.
5. Kharitonenkov, A., Z. Chen, I. Sures, H. Wang, J. Schilling, and A. Ullrich. 1997. A family of proteins that inhibit signalling through tyrosine kinase receptors. *NatuSe* 386: 181–186.
6. Van Beek, E. M., F. Cochrane, A. N. Barclay, and T. K. van den Berg. 2005. Signal regulatory proteins in the immune system. *J. Immunol.* 175: 7781–7787.
7. Ohnishi, H., M. Kubota, A. Ohtake, K. Sato, and S. Sano. 1996. Activation of protein-tyrosine phosphatase SH-PTP2 by a tyrosine-based activation motif of a novel brain molecule. *J. Biol. Chem.* 271: 25569–25574.
8. Timms, J. F., K. Carlberg, H. Gu, H. Chen, S. Kamatkar, M. J. Nadler, L. R. Rohrschneider, and B. G. Neel. 1998. Identification of major binding proteins and substrates for the SH2-containing protein tyrosine phosphatase SHP-1 in macrophages. *Mol. Cell. Biol.* 18: 3838–3850.
9. Oshima, K., A. R. Ruhul Amin, A. Suzuki, M. Hamaguchi, and S. Matsuda. 2002. SHPS-1, a multifunctional transmembrane glycoprotein. *FEB4 Lett.* 519: 1–7.
10. Jiang, P., C. F. Lagenaur, and V. Narayanan. 1999. Integrin-associated protein is a ligand for the P84 neural adhesion molecule. *J. Biol. Chem.* 274: 559–562.
11. Seiffert, M., C. Cant, Z. Chen, I. Rappold, W. Brugger, L. Kanz, E. J. Brown, A. Ullrich, and H. J. Buhring. 1999. Human signal-regulatory protein is expressed on normal, but not on subsets of leukemic myeloid cells and mediates cellular adhesion involving its counterreceptor CD47. *Blood* 94: 3633–3643.
12. Brown, E. J., and W. A. Frazier. 2001. Integrin-associated protein (CD47) and its ligands. *TSendT Cell Biol.* 11: 130–135.
13. Adams, S., L. J. van der Laan, E. Vernon-Wilson, C. Renardel de Lavalette, E. A. Dopp, C. D. Dijkstra, D. L. Simmons, and T. K. van den Berg. 1998. Signal-regulatory protein is selectively expressed by myeloid and neuronal cells. *J. Immunol.* 161: 1853–1859.
14. Veillette, A., E. Thibaudeau, and S. Latour. 1998. High expression of inhibitory receptor SHPS-1 and its association with protein-tyrosine phosphatase SHP-1 in macrophages. *J. Biol. Chem.* 273: 22719–22728.
15. Latour, S., H. Tanaka, C. Demeure, V. Mateo, M. Rubio, E. J. Brown, C. Maliszewski, F. P. Lindberg, A. Oldenborg, A. Ullrich, et al. 2001. Bidirectional negative regulation of human T and dendritic cells by CD47 and its cognate receptor signal-regulator protein- : down-regulation of IL-12 responsiveness and inhibition of dendritic cell activation. *J. Immunol.* 167: 2547–2554.
16. Seiffert, M., P. Brossart, C. Cant, M. Cella, M. Colonna, W. Brugger, L. Kanz, A. Ullrich, and H. J. Buhring. 2001. Signal-regulatory protein (SIRP) but not SIRP is involved in T-cell activation, binds to CD47 with high affinity, and is expressed on immature CD34 CD38 hematopoietic cells. *Blood* 97: 2741–2749.
17. Oldenborg, P. A., A. Zheleznyak, Y. F. Fang, C. F. Lagenaur, H. D. Gresham, and F. P. Lindberg. 2000. Role of CD47 as a marker of self on red blood cells. *4cience* 288: 2051–2054.
18. Okazawa, H., S. Motegi, N. Ohyama, H. Ohnishi, T. Tomizawa, Y. Kaneko, P. A. Oldenborg, O. Ishikawa, and T. Matozaki. 2005. Negative regulation of phagocytosis in macrophages by the CD47-SHPS-1 system. *J. Immunol.* 174: 2004–2011.
19. Ishikawa-Sekigami, T., Y. Kaneko, H. Okazawa, T. Tomizawa, J. Okajo, Y. Saito, C. Okuzawa, M. Sugawara-Yokoo, U. Nishiyama, H. Ohnishi, et al. 2006. SHPS-1 promotes the survival of circulating erythrocytes through inhibition of phagocytosis by splenic macrophages. *Blood* 107: 341–348.
20. Alblas, J., H. Honing, C. R. de Lavalette, M. H. Brown, C. D. Dijkstra, and T. K. van den Berg. 2005. Signal regulatory protein ligation induces macrophage nitric oxide production through JAK/STAT- and phosphatidylinositol 3-kinase/Rac1/NAPDH oxidase/H_2O_2-dependent pathways. *Mol. Cell. Biol.* 25: 7181–7192.
21. Inagaki, K., T. Yamao, T. Noguchi, T. Matozaki, K. Fukunaga, T. Takada, T. Hosooka, S. Akira, and M. Kasuga. 2000. SHPS-1 regulates integrin-mediated cytoskeletal reorganization and cell motility. *EMBO J.* 19: 6721–6731.
22. Chang, T. T., C. Jabs, R. A. Sobel, V. K. Kuchroo, and A. H. Sharpe. 1999. Studies in B7-deficient mice reveal a critical role for B7 costimulation in both induction and effector phases of experimental autoimmune encephalomyelitis. *J. Exp. Med.* 190: 733–740.
23. Bakker, A. B., R. M. Hoek, A. Cerwenka, B. Blom, L. Lucian, T. McNeil, R. Murray, L. H. Phillips, J. D. Sedgwick, and L. L. Lanier. 2000. DAP12-deficient mice fail to develop autoimmunity due to impaired antigen priming. *Immunity* 13: 345–353.
24. Chitnis, T., N. Najafian, C. Benou, A. D. Salama, M. J. Grusby, M. H. Sayegh, and S. J. Khoury. 2001. Effect of targeted disruption of STAT4 and STAT6 on the induction of experimental autoimmune encephalomyelitis. *J. Clin. InveTl.* 108: 739–747.
25. Fukao, T., S. Matsuda, and S. Koyasu. 2000. Synergistic effects of IL-4 and IL-18 on IL-12-dependent IFN- production by dendritic cells. *J. Immunol.* 164: 64–71.
26. Fukao, T., D. M. Frucht, G. Yap, M. Gadina, J. J. O'Shea, and S. Koyasu. 2001. Inducible expression of Stat4 in dendritic cells and macrophages and its critical role in innate and adaptive immune responses. *J. Immunol.* 166: 4446–4455.
27. Fang, D., C. Elly, B. Gao, N. Fang, Y. Altman, C. Joazeiro, T. Hunter, N. Copeland, N. Jenkins, and Y. C. Liu. 2002. Dysregulation of T lymphocyte

function in itchy mice: a role for itch in T$_H$2 differentiation. *Nat. Immunol.* 3: 281o287.
28. Kumanogoh, A., T. Shikina, K. Suzuki, S. Uematsu, K. Yukawa, S. Kashiwamura, H. Tsutsui, M. Yamamoto, H. Takamatsu, E. P. Ko-Mitamura, et al. 2005. Nonredundant roles of Sema4A in the immune system: defective T cell priming and Th1/Th2 regulation in Sema4A-deficient mice. *Immunity* 22: 305o316.
29. Li, M., G. M. Davey, R. M. Sutherland, C. Kurts, A. M. Lew, C. Hirst, F. R. Carbone, and W. R. Heath. 2001. Cell-associated ovalbumin is cross-presented much more efficiently than soluble ovalbumin in vivo. *J. Immunol.* 166: 6099o6103.
30. Fukao, T., M. Tanabe, Y. Terauchi, T. Ota, S. Matsuda, T. Asano, T. Kadowaki, T. Takeuchi, and S. Koyasu. 2002. PI3K-mediated negative feedback regulation of IL-12 production in DCs. *Nat. Immunol.* 3: 875o881.
31. Ujike, A., K. Takeda, A. Nakamura, S. Ebihara, K. Akiyama, and T. Taki. 2002. Impaired dendritic cell maturation and increased T$_H$2 responses in PIR-B $^{-/-}$ mice. *Nat. Immunol.* 3: 542o548.
32. Pedotti, R., J. J. De Voss, L. Steinman, and S. J. Galli. 2003. Involvement of both Allergic' and Autoimmune' mechanisms in EAE, MS and other autoimmune diseases. *TSendT Immunol.* 24: 479o484.
33. Sospedra, M., and R. Martin. 2005. Immunology of multiple sclerosis. *Annu. Rev. Immunol.* 23: 683o747.
34. Park, H., Z. Li, 9. O. Yang, S. H. Chang, R. Nurieva, Y. H. Wang, Y. Wang, L. Hood, Z. Zhu, 2. Tian, and C. Dong. 2005. A distinct lineage of CD4 T cells regulates tissue inflammation by producing interleukin 17. *Nat. Immunol.* 6: 1133o1141.
35. Bettelli, E., Y. Carrier, W. Gao, T. Korn, T. B. Strom, M. Oukka, H. L. Weiner, and V. K. Kuchroo. 2006. Reciprocal developmental pathways for the generation of pathogenic effector T$_H$17 and regulatory T cells. *NatuSe* 441: 235o238.
36. Komiyama, Y., S. Nakae, T. Matsuki, A. Nambu, H. Ishigame, S. Kakuta, K. Sudo, and Y. Iwakura. 2006. IL-17 plays an important role in the development of experimental autoimmune encephalomyelitis. *J. Immunol.* 177: 566o573.
37. Barnden, M. J., J. Allison, W. R. Heath, and F. R. Carbone. 1998. Defective TCR expression in transgenic mice constructed using cDNA-based - and -chain genes under the control of heterologous regulatory elements. *Immunol. Cell Biol.* 76: 34o40.
38. Frucht, D. M., T. Fukao, C. Bogdan, H. Schindler, J. J. O'Shea, and S. Koyasu. 2001. IFN- production by antigen-presenting cells: mechanisms emerge. *TSendT Immunol.* 22: 556o560.
39. Oldenborg, P. A., H. D. Gresham, and F. P. Lindberg. 2001. CD47-signal regulatory protein (SIRP) regulates Fc and complement receptor-mediated phagocytosis. *J. Exp. Med.* 193: 855o862.
40. Watford, W. T., B. D. Hissong, J. H. Bream, Y. Kanno, L. Muul, and J. J. O'Shea. 2004. Signaling by IL-12 and IL-23 and the immunoregulatory roles of STAT4. *Immunol. Rev.* 202: 139o156.
41. Gadina, M., L. M. Stancato, C. M. Bacon, A. C. Larner, and J. J. O'Shea. 1998. Involvement of SHP-2 in multiple aspects of IL-2 signaling: evidence for a positive regulatory role. *J. Immunol.* 160: 4657o4661.
42. Ndhlovu, L. C., N. Ishii, K. Murata, T. Sato, and K. Sugamura. 2001. Critical involvement of O9 40 ligand signals in the T cell priming events during experimental autoimmune encephalomyelitis. *J. Immunol.* 167: 2991o2999.
43. Hagnerud, S., P. P. Manna, M. Cella, A. Stenberg, W. A. Frazier, M. Colonna, and P. A. Oldenborg. 2006. Deficit of CD47 results in a defect of marginal zone dendritic cells, blunted immune response to particulate antigen and impairment of skin dendritic cell migration. *J. Immunol.* 176: 5772o5778.
44. Fukunaga, A., H. Nagai, 9. Yu, S. Oniki, H. Okazawa, S. Motegi, R. Suzuki, N. Honma, T. Matozaki, C. Nishigori, and T. Horikawa. 2006. Src homology 2 domain-containing protein tyrosine phosphatase substrate 1 regulates the induction of Langerhans cell maturation. *EuS J. Immunol.* 36: 3216o3226.
45. Reinhold, M. I., F. P. Lindberg, G. J. Kersh, P. M. Allen, and E. J. Brown. 1997. Costimulation of T cell activation by integrin-associated protein (CD47) is an adhesion-dependent, CD28-independent signaling pathway. *J. Exp. Med.* 185: 1o11.
46. Greter, M., F. L. Heppner, M. P. Lemos, B. M. Odermatt, N. Goebels, T. Laufer, R. J. Noelle, and B. Becher. 2005. Dendritic cells permit immune invasion of the CNS in an animal model of multiple sclerosis. *Nat. Med.* 11: 328o334.
47. Heppner, F. L., M. Greter, D. Marino, J. Falsig, G. Raivich, N. Hovelmeyer, A. Waisman, T. Rulicke, M. Prinz, J. Priller, et al. 2005. Experimental autoimmune encephalomyelitis repressed by microglial paralysis. *Nat. Med.* 11: 146o152.

PERGAMON

Neuromuscular Disorders xxx (2007) xxx–xxx

www.elsevier.com/locate/nmd

Novel homozygous mutation of the caveolin-3 gene in rippling muscle disease with extraocular muscle paresis

H. Ueyama [a,b,*], H. Horinouchi [a,c], K. Obayashi [a,d], M. Hashinaga [a], T. Okazaki [a], T. Kumamoto [a]

[a] *Division of Neurology and Neuromuscular Disorders, Department of Brain and Nerve Science, Oita University Faculty of Medicine, Hasama-machi, Yufu City, Oita 879-5593, Japan*

[b] *Department of Neurology, Kumamoto Saishunso Hospital, National Hospital Organization, 2659 Suya, Koshi City, Kumamoto 861-1102, Japan*

[c] *Department of Neurology, Nagato Memorial Hospital, Tsuruoka 1-11-59, Saiki City, Oita 876-0835, Japan*

[d] *Department of Diagnostic Medicine, Graduate School of Medical Sciences, Kumamoto University, Honjo 1-1-1, Kumamoto City, Kumamoto 860-0811, Japan*

Received 4 September 2006; received in revised form 12 December 2006; accepted 15 March 2007

Abstract

We describe a 39-year-old Japanese man with rippling muscle disease who carried a novel homozygous mutation (Trp70 to a stop codon) in the caveolin-3 gene. The patient also had extraocular muscle paresis showing atrophy of the extraocular muscles on orbital MRI. The involvement of the extraocular muscles of patients with caveolinopathy is discussed.

Keywords: Rippling muscle disease; Caveolin-3; Homozygote; Extraocular muscle; Limb-girdle muscular dystrophy 1C

1. Introduction

Rippling muscle disease is characterized by the involuntary rolling contractions of muscles that occur on mechanical stretching [1]. Most cases are regarded as one phenotype of caveolinopathy due to mutations in the caveolin-3 gene (CAV3) on chromosome 3p25 [2,3]. In general, extraocular muscles are spared. Here, we report a Japanese patient with the disease having extraocular muscle paresis. Molecular analysis revealed that the patient had a novel homozygous nonsense mutation in the CAV3 and the asymptomatic mother was heterozygote, suggesting an autosomal recessive mode of inheritance.

* Corresponding author. Address: Department of Neurology, Kumamoto Saishunso Hospital, National Hospital Organization, 2659 Suya, Koshi City, Kumamoto 861-1102, Japan. Tel.: +81 96 242 1000; fax: +81 96 249 1900.

E-mail address: hueyama@saisyunsou1.hosp.go.jp (H. Ueyama).

0960-8966/$ - see front matter © 2007 Elsevier B.V. All rights reserved.
doi:10.1016/j.nmd.2007.03.009

2. Case report

A 39-year-old man was healthy until age 9 when he noted hypertrophy of the calf muscles, muscle cramps after running, and rolling contraction after stretching the femoral muscle suddenly. At age 13, he complained of muscle stiffness after walking for extended periods. On April 18, 2005, he experienced abdominal muscle pain after playing tennis. Elevated serum CK level was identified by his local doctor, and he was referred to our hospital. The family history for neuromuscular diseases was unremarkable. On admission, the patient was a well-developed man with hypertrophy of the calf muscles. He had mild blepharoptosis, and extraocular movement revealed bilateral upward and lateral gaze limitation without diplopia (Fig. 1). His muscle power was normal except for mild weakness of the bilateral adductor thigh muscle. A peculiar rippling movement in the quadriceps or biceps muscles,

Please cite this article in press as: Ueyama H et al., Novel homozygous mutation of the caveolin-3 gene ..., Neuromuscul Disord (2007), doi:10.1016/j.nmd.2007.03.009

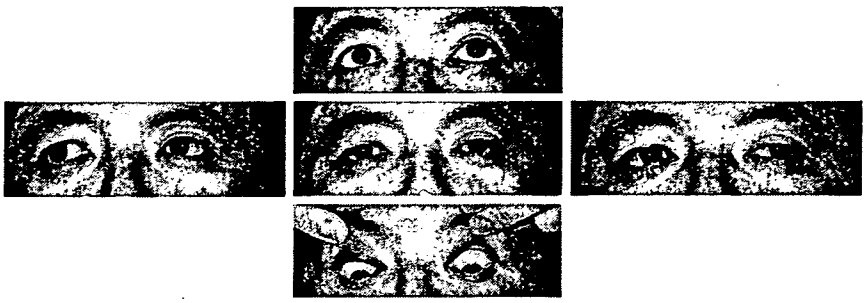

Fig. 1. Extraocular movement of the patient. He shows bilateral upward and lateral gaze limitation.

mounding phenomenon, and percussion-induced rapid muscle contraction was seen. Routine laboratory tests were all normal except for an elevated serum CK level (729 IU/L; normal <160). Electrocardiogram and cardiac sonogram were normal, and tensilon test and anti-acetylcholine receptor antibody were negative. Nerve conduction studies, repetitive nerve stimulation, and needle electromyography were normal, and no myotonic discharges were elicited. Skeletal muscle MRI of the lower limbs demonstrated decreased density and size in the bilateral gracillis, biceps femoris, and tibialis anterior muscles (Fig. 2a and b). Ophthalmologic tests revealed a normal Hess chart, visual field, and optic fundus. Orbital MRI showed atrophy of the bilateral superior and lateral rectus muscles (Fig. 2c and d). Muscle biopsy from the left biceps brachii showed mild myopathic changes without cellular response, group atrophy, or ragged-red fibers.

3. Methods

3.1. Immunohistochemistry

Eight micrometer thick cryostat biopsied muscle sections were fixed in acetone for 10 min. After blocking with phosphate-buffered saline containing 10% (W/V) nonfat dry milk, each section was incubated with 1:200 diluted monoclonal antibody against human caveolin-3 (BD Transduction Laboratories, Lexington, KY) for 1 h at room temperature. After washing, biotinylated goat anti-mouse IgG was added for 30 min. The sections were incubated in avidin–biotin–peroxidase complex (Vectastain ABC kit, Vector Labs) for 30 min, and visualized with 3, 3′-diaminobenzidine tetrahydrochloride.

3.2. Molecular analyses

After informed consent had been obtained from the family members, genomic DNA was extracted from peripheral blood mononuclear cells by standard procedures. Two coding exons of the caveolin-3 gene were amplified by PCR according to the method of McNally and associates [4]. Refined PCR products were directly sequenced with an ABI 310 fluorescent sequencer (Applied Biosystems, Tokyo, Japan). The mutation was confirmed by analysis of the PCR product by restriction enzyme digestion with *Spe*I.

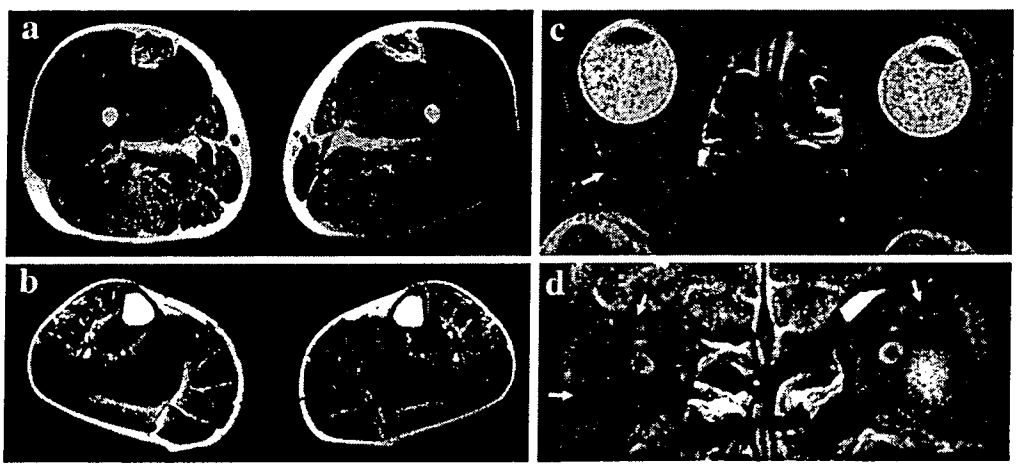

Fig. 2. T2-weighted skeletal muscle MRI of the lower limbs demonstrates areas of high signal intensity and mild atrophy in the bilateral gracillis, biceps femoris, and tibialis anterior muscles. (a) Thigh medial level, (b) leg medial level. T2-weighted, fat-suppressed orbital MRI shows atrophy of the bilateral superior and lateral rectus muscles (arrows). (c) Horizontal section, (d) coronal section.

Please cite this article in press as: Ueyama H et al., Novel homozygous mutation of the caveolin-3 gene ..., Neuromuscul Disord (2007), doi:10.1016/j.nmd.2007.03.009

4. Results

Immunohistochemical analysis revealed a complete absence of caveolin-3 protein expression in the patient's skeletal muscle sarcolemma (data not shown). Sequence analysis of the caveolin-3 gene revealed that the patient had a homozygous substitution of guanine (G) to adenine (A), changing tryptophan (Trp) to stop codon at codon 70 of the caveolin-3 gene (data not shown). The patient's mother showed a heterozygous substitution at this position. As this mutation creates a novel restriction enzyme site with *Spe*I, genotype analysis of the family members confirmed that the patient was homozygous and the mother was heterozygous (Fig. 3). As the father was dead, DNA analysis was not available. Careful neurologic examination of the mother was normal. We did not detect this mutation in 50 normal Japanese control subjects.

5. Discussion

Rippling muscle disease is a rare skeletal muscle disorder, characterized by a unique rippling movement, mounding phenomenon, percussion-induced rapid muscle contraction, and hyperCKemia [1,3]. Most cases show a decreased expression of caveolin-3 protein in the biopsied muscle, and CAV3 is mutated [2]. Our patient fulfilled the above characteristic features except for extraocular muscle involvement.

We found a novel homozygous mutation in the CAV3, which substituted codon 70 Trp with a stop codon. This alteration is located in the scaffolding domain of the caveolin-3 protein, and affects amino acids conserved in humans, rats, and mice [4]. As the asymptomatic mother was heterozygous for this mutation, we speculate that the mode of inheritance was autosomal recessive. The majority of caveolinopathy patients have autosomal-dominant inheritance, and recessive inheritance is extremely rare [5–8]. Only A92T and splice site mutation were seen in a genetically confirmed patient with recessive inheritance [7,8].

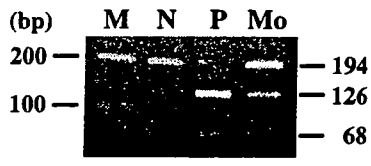

Fig. 3. Allele-specific restriction enzyme digestion with *Spe*I. In the presence of the mutation, a 194 bp PCR fragment from exon 2 of the caveolin-3 gene is cut into two fragments of 126 and 68 bp. The mutation was not observed in a normal control (N), showing only an uncut fragment (194 bp). The patient (P) showed two cut fragments (126 and 68 bp), demonstrating a homozygote in this position. The mother (Mo) showed a mixed pattern, demonstrating a heterozygote. M, size marker.

It was reported that the homozygous caveolinopathy patients presented with a more severe clinical phenotype than the usually seen in rippling muscle disease [6,7]. However, our patient showed no clinical difference with the heterozygous patients without complications such as short stature, cardiac involvement, delayed bone age, or permanent muscle stiffness as reported previously [5]. A possible explanation may be related to the different mutations, depending on the dominant negative effect of the mutations on its protein product [9]. Interestingly, it is known that caveolin-3-deficient mice by targeting exon 2 are also inherited through the recessive form [10].

The most important symptom of our patient was extraocular muscle paresis. As the oculocephalic reflex was negative and orbital MRI demonstrated atrophy of the extraocular muscles, we speculated that his extraocular muscles were involved. We could find no other causes of limited gaze in the patient such as myasthenia gravis, dysthyroid opthalmopathy, ocular myositis, Duane's syndrome, or mitochondrial myopathy. The atrophy of both extraocular and skeletal muscles demonstrated by MRI allows us to suppose the same etiology. In general, caveolinopathy does not induce extraocular muscle paresis, but only one patient has been reported in the literature [11]. The authors considered that the patient had a rippling phenomenon of the extraocular muscle; however, myasthenia gravis was later diagnosed in this patient. By contrast, our patient seemed to have a different pathomechanism, because he did not show any transient diplopia or amelioration by palpebration. Further genetic and clinical studies are necessary to demonstrate whether this symptom is only related to caveolinopathy.

References

[1] Torbergsen T. Rippling muscle disease: a review. Muscle Nerve 2002(Suppl. 11):S103–7.
[2] Betz RC, Schoser BG, Kasper D, et al. Mutations in CAV3 cause mechanical hyperirritability of skeletal muscle in rippling muscle disease. Nat Genet 2001;28:218–9.
[3] Woodman SE, Sotgia F, Galbiati F, Minetti C, Lisanti MP. Caveolinopathies. Mutations in caveolin-3 cause four distinct autosomal dominant muscle diseases. Neurology 2004;62: 538–43.
[4] McNally EM, Moreira E, Duggan DJ, et al. Caveolin-3 in muscular dystrophy. Hum Mol Genet 1998;7:871–7.
[5] Koul RL, Chand RP, Chacko A, et al. Severe autosomal recessive rippling muscle disease. Muscle Nerve 2001;24: 1542–7.
[6] Kubisch C, Schoser BG, von Düring M, et al. Homozygous mutations in caveolin-3 cause a severe form of rippling muscle disease. Ann Neurol 2003;53:512–20.
[7] Kubisch C, Ketelsen UP, Goebel I, Omran H. Autosomal recessive rippling muscle disease with homozygous CAV3 mutations. Ann Neurol 2005;57:303–4.

Please cite this article in press as: Ueyama H et al., Novel homozygous mutation of the caveolin-3 gene ..., Neuromuscul Disord (2007), doi:10.1016/j.nmd.2007.03.009

[8] Müller JS, Piko H, Schoser BGH, et al. Novel splice site mutation in the caveolin-3 gene leading to autosomal recessive limb girdle muscular dystrophy. Neuromuscul Disord 2006;16:432–6.

[9] Minetti C, Sotgia F, Bruno C, et al. Mutations in the caveolin-3 gene cause autosomal dominant limb-girdle muscular dystrophy. Nat Genet 1998;18:365–8.

[10] Hagiwara Y, Sasaoka T, Araishi K, et al. Caveolin-3 deficiency causes muscle degeneration in mice. Hum Mol Genet 2000;9:3047–54.

[11] Kosmorsky GS, Mehta N, Mitsumoto H, Prayson R. Intermittent esotropia associated with rippling muscle disease. J Neuroopthalmol 1995;15:147–51.

Please cite this article in press as: Ueyama H et al., Novel homozygous mutation of the caveolin-3 gene..., Neuromuscul Disord (2007), doi:10.1016/j.nmd.2007.03.009

JOURNAL OF CLINICAL MICROBIOLOGY, May 2007, p. 1426–1432 Vol. 45, No. 5
0095-1137/07/$08.00+0 doi:10.1128/JCM.01515-06

Simultaneous Quantification of Epstein-Barr Virus, Cytomegalovirus, and Human Herpesvirus 6 DNA in Samples from Transplant Recipients by Multiplex Real-Time PCR Assay[▽]

Kaoru Wada,[1] Naomi Kubota,[1] Yoshinori Ito,[2] Hiroshi Yagasaki,[2] Koji Kato,[3] Tetsushi Yoshikawa,[4] Yasuyuki Ono,[5] Hisami Ando,[5] Yasuhiro Fujimoto,[6] Tetsuya Kiuchi,[6] Seiji Kojima,[2] Yukihiro Nishiyama,[1] and Hiroshi Kimura[1]*

Departments of Virology,[1] Pediatrics,[2] Pediatric Surgery,[5] and Transplant Surgery,[6] Nagoya University Graduate School of Medicine, Nagoya, Japan; Department of Pediatrics, Japanese Red Cross Nagoya First Hospital, Nagoya, Japan[3]; and Department of Pediatrics, Fujita Health University School of Medicine, Toyoake, Japan[4]

Received 22 July 2006/Returned for modification 31 October 2006/Accepted 12 March 2007

We developed a multiplex real-time PCR assay using 6-carboxyfluorescein, 6-carboxy-4′,5′-dichloro-2′,7′-dimethoxyfluorescein, and carbocyanine 5-labeled probes to simultaneously quantify Epstein-Barr virus (EBV), cytomegalovirus (CMV), and human herpesvirus 6 (HHV-6) DNA. When previously tested and stored DNA samples were examined, results of the multiplex real-time PCR assay were as sensitive and specific as those of a single real-time PCR assay. The multiplex assay was used to quantify the EBV, CMV, and HHV-6 DNA in 46 transplant recipients. A total of 303 whole-blood and plasma specimens were collected and analyzed. According to the results of the multiplex assay, the detection rates for viral DNA in whole blood and plasma were 23.8% and 5.9% for EBV, 11.2% and 5.3% for CMV, and 12.5% and 2.0% for HHV-6, respectively. All forms of viral DNA were detected more frequently in whole blood than in plasma. During the symptomatic period, EBV DNA was detected in all whole-blood specimens but not in all plasma specimens. Furthermore, the EBV DNA load in whole blood was higher during the symptomatic period than during the asymptomatic period, whereas the EBV DNA load in plasma was similar for both periods. These results demonstrate that whole blood is more suitable for the quantification of EBV DNA in transplant patients. However, a cutoff value with clinical relevance still needs to be determined.

Herpesviruses are ubiquitous in the human population and often become reactivated in latently infected immunocompromised patients (4, 22). Herpesvirus reactivation frequently occurs after hematopoietic stem cell or solid-organ transplantation and occasionally results in symptomatic diseases (2, 4, 28). Among human herpesviruses, Epstein-Barr virus (EBV), cytomegalovirus (CMV), and human herpesvirus 6 (HHV-6) may cause life-threatening complications, such as lymphoproliferative disorders (3, 13, 27), interstitial pneumonia (7, 15), and encephalitis (2, 12, 23, 25). Therefore, to ensure the success of transplantation, it is essential to monitor for these viruses and diagnose any virus-related diseases as early as possible.

With the advent of real-time PCR technology, quantitative PCR assays are becoming widespread methodologies for diagnostic purposes (9, 11). We initially developed quantitative real-time PCR systems to detect EBV (5), CMV (18), and HHV-6 DNA (19). However, because each system was able to detect only one form of viral DNA, simultaneous virus monitoring was cost, time, and labor intensive. It was recently shown that quantification of more than one target per well is possible with the use of different fluorochromes (1, 14, 21, 24). One aim of the present study was to establish a system for the simultaneous quantification of EBV, CMV, and HHV-6 DNA by using a multiplex real-time PCR assay. Another goal was to identify specimens that would optimize virus monitoring. While peripheral blood cells, whole blood, and plasma are commonly used in quantitative real-time PCR, whole blood and plasma are more convenient to use and are suitable for clinical analysis. Since whole blood contains peripheral blood cells, we considered that whole blood could be used instead of peripheral blood cells. In the present study, we developed a multiplex real-time PCR assay to quantify EBV, CMV, and HHV-6 DNA. In addition, we sought to determine whether whole blood or plasma was more suitable for simultaneous virus monitoring in samples from transplant recipients.

MATERIALS AND METHODS

Patients and clinical specimens. In total, 27 hematopoietic stem cell transplantation recipients (16 men, 11 women) and 19 liver transplantation recipients (9 men, 10 women) were enrolled in the study. Beginning 1 week after transplantation, EDTA blood samples were prospectively obtained from subjects weekly until they were discharged. From 46 patients, 1 to 13 samples per patient (total 303, mean 6.6) were collected from 1 to 15 weeks after transplantation (mean 7.8 weeks). From some patients, only a few samples could be obtained because of their early death or follow-up loss. Informed consent was obtained from all patients or guardians. The institutional review board of Nagoya University Hospital approved the use of specimens included in this study.

Among the hematopoietic stem cell transplantation recipients, 10 had acute leukemia, 6 had severe aplastic anemia, 4 had solid tumors, 2 had chronic leukemia, and 5 had other diseases. The patients underwent transplantation between November 2003 and October 2005 at Nagoya University Hospital or at Japanese Red Cross Nagoya First Hospital. The median age of the patients was 8.0 years (range, 1 to 22 years). Eight of 27 patients received antithymocyte globulin, which is known to be a risk factor for EBV-related lymphoproliferative disorders (3, 13).

* Corresponding author. Mailing address: Department of Virology, Nagoya University Graduate School of Medicine, 65 Tsuruma-cho, Showa-ku, Nagoya 466-8550, Japan. Phone: 81-52-744-2207. Fax: 81-52-744-2452. E-mail: hkimura@med.nagoya-u.ac.jp.

▽ Published ahead of print on 21 March 2007.

TABLE 1. Sequences of primers and probes used in the real-time PCR assay

Target gene (GenBank accession no.)	Primer or probe	Sequence (5′→3′)[a]	Genome coordinate
EBV BALF5 (AJ507799)	Forward primer	CGGAAGCCCTCTGGACTTC	156007–156025
	Reverse primer	CCCTGTTTATCCGATGGAATG	155936–55956
	Probe	FAM-TGTACACGCACGAGAAATGCGCC-BHQ1a	155959–155981
CMV IE (NC001347)	Forward primer	GACTAGTGTGATGCTGGCCAAG	172435–172456
	Reverse primer	GCTACAATAGCCTCTTCCTCATCTG	172256–172270
	Probe	JOE-AGCCTGAGGTTATCAGTGTAATGAAGCGCC-BHQ1a	172389–172418
HHV-6 U31 (AF157706)	Forward primer	TTTGCAGTCATCACGATCGG	46661–46680
	Reverse primer	AGAGCGACAAATTGGAGGTTTC	46862–46883
	Probe	Cy5-AGCCACAGCAGCCATCTACATCTGTCAA-BHQ3a	46753–46780

[a] FAM, 6-carboxyfluorescein; JOE, 6-carboxy-4′,5′-dichloro-2′,7′-dimethoxyfluorescein; Cy5, carbocyanine 5.

The liver transplantation recipients received their organs from living donors at Nagoya University Hospital between February 2004 and December 2005. Of 19 patients, 8 had hepatic cirrhosis (hepatitis B virus, 3; hepatitis C virus, 2; other viruses, 3), 3 had biliary atresia, and 8 had other diseases. The median age of the patients was 48.0 years (range, 6 months to 62 years).

Symptomatic EBV infections were diagnosed from clinical findings (fever, enlarged lymph nodes, and hematochezia) and serological examinations. A lymph node biopsy provided histological confirmation that one patient with symptomatic EBV infection had posttransplant lymphoproliferative disorder. CMV hepatitis was diagnosed from the clinical findings and serological examination and confirmed by liver biopsy.

A total of 303 consecutive blood specimens were obtained from transplant recipients and divided into whole-blood or plasma samples, and the 303 paired samples were tested with the multiplex real-time PCR assay. Viral DNA was extracted from 200 μl of whole blood or 200 μl of plasma, using QIAamp DNA blood kits (QIAGEN, Hilden, Germany) and eluted in 100 μl of water.

Specificity and sensitivity studies were performed with 111 DNA samples that had been obtained from other transplantation recipients. These DNA samples had been extracted from either whole-blood or plasma samples and used to monitor viruses by either qualitative PCR or real-time PCR, and stored at −30°C.

The specificity was also confirmed with viral DNA from standard strains (KOS for herpes simplex virus type 1, 186 for herpes simplex virus type 2, Kawaguchi strain for varicella-zoster virus, B95-8 for EBV, AD169 for CMV, Sato strain for HHV-7, and a clinical isolate from a patient with exanthem subitum for HHV-6). Viral DNA was extracted from the supernatant of each virus culture and was used for the cross-reactivity study.

EDTA blood was taken from a patient who was seronegative for EBV, CMV, and HHV-6, and plasma was separated. A DNA extraction solution from either the whole blood or the plasma fraction was used for reconstruction studies.

Primers and probes. The sequences of the primers and probes used for the multiplex real-time PCR assay are listed in Table 1. The primer and probe sets for the viruses have been described previously (5, 18, 19). Each probe was labeled with different fluorochromes, as follows: the EBV probe was labeled with 6-carboxyfluorescein and quenched with Black-Hole-Quencher 1a (BHQ1a); the CMV probe was labeled with 6-carboxy-4′,5′-dichloro-2′,7′-dimethoxyfluorescein and quenched with BHQ1a; the HHV-6 probe was labeled with carbocyanine 5 and quenched with BHQ3a. All primers (Fasmac, Kanagawa, Japan) and probes (Operon Biotechnologies, Huntsville, AL) were synthesized commercially.

Quantification of viral DNA by multiplex real-time PCR. Multiplex and independent real-time PCR were performed with a QuantiTect multiplex PCR kit (QIAGEN). The multiplex real-time PCR assay was performed in a total reaction mixture (25 μl) containing 5 μl of DNA extracts, 12.5 μl of 2× QuantiTect multiplex PCR master mix, each forward and reverse primer, and each probe. To determine the optimal concentrations of the primers and probes, we evaluated various concentrations of primer and probe sets using the multiplex real-time PCR assay. The optimal concentration of forward primer was 200 nM for EBV and 100 nM for CMV and HHV-6. The optimal concentration of reverse primer was 200 nM for EBV, 100 nM for CMV, and 200 nM for HHV-6. The optimal concentration of each probe was 100 nM. The independent real-time PCR was performed in the same way as the multiplex real-time PCR assay except that only one primer/probe set was included. Amplification and real-time fluorescence detection were performed with a model Mx3000P real-time PCR system (Stratagene, La Jolla, CA) using the following protocol: an initial denaturation and polymerase activation step for 15 min at 95°C, followed by 50 cycles of denaturation at 95°C for 15 s and 60°C for 1 min. Real-time fluorescence measurements were taken, and a threshold cycle value for each sample was calculated by determining the point at which the fluorescence exceeded a threshold limit. Each real-time PCR assay contained the dilution series of a standard for the calibration curve, and all samples and the standard were run in duplicate. The standards were plasmid controls that contained the PCR products amplified by each primer set, as described previously (5, 18, 19). For the multiplex real-time PCR, each plasmid control was mixed, diluted, and used to make calibration curves. The number of viral DNA copies was calculated from the standard curves and expressed as copies per 1 ml of whole blood or plasma.

CMV antigenemia assay. The CMV antigenemia assay was performed as previously described (18). The approximate antigenemia threshold was 1 positive cell per 5×10^4 leukocytes, as determined by guidelines from the Japanese Society for Hematopoietic Cell Transplantation. When the antigenemia assay was positive, patients were administered ganciclovir preemptively.

Statistical analysis. StatView J 4.02 (Abacus Concepts Inc., Berkeley, CA) was used to perform the data analysis. A regression analysis compared the multiplex assay with the single assay. Fisher's exact test was used to compare the viral DNA detection rates, and Student's t test was used to compare the mean viral DNA $\log_{10}$ copy numbers. To determine the minimum detection level of each assay, 35 replicates each of one, two, and five copies of the plasmid standard were quantified. The 95% confidence interval (CI) was calculated from the t distribution using the following formula: 95% CI = the mean of the estimated copy number $\pm t \times$ standard error, where t was estimated to be 2.042 from the Student's t table.

RESULTS

Specificity and sensitivity of the multiplex quantification using an Mx3000P real-time PCR system. Serial dilutions of mixed viral standard plasmids were tested with the multiplex assay, and three standard curves were constructed from the cycle of threshold values. The assay was able to detect each viral DNA form over a linear span between 5 and 5×10^6 copies per reaction mixture without interference (Fig. 1). The standard curves generated from the multiplex real-time PCR were almost equal to those generated from the single assay. Because amplification efficiency may be influenced by the background DNA of the clinical specimen, we evaluated the performance of the multiplex assay using standard plasmids diluted in water or in water containing EBV-, CMV-, and HHV-6-negative human genomic DNA. The standard curves generated from the standard plasmids in background DNA were almost equal to those generated from the standard plasmids in water, indicating that amplification efficiency was not influenced by the background DNA (data not shown). We also performed reconstruction studies to confirm the absence of the